Electromagnetic wave propagation in spatiotemporally varying Drude metamaterials

by

Krish Nigam

Thesis Supervisors:

Dr T. V. Raziman
Prof. Richard V. Craster

Submitted to the Department of Mathematics
in partial fulfillment of the requirements for the degree of

MASTER OF SCIENCE IN MATHEMATICS

at

IMPERIAL COLLEGE LONDON
OF SCIENCE TECHNOLOGY AND MEDICINE

June 2025

The work contained in this thesis is my own work unless otherwise stated.

Signed: Krish Nigam Date: June 9, 2025

Abstract

This thesis investigates the propagation of electromagnetic plane waves through spatiotemporally modulated Drude metamaterials, with a focus on systems exhibiting periodicity in both space and time, a class of materials known as space-time crystals. Motivated by recent interest in dynamically tunable media and their exotic wave phenomena, we develop a theoretical framework to understand how a travelling-wave temporal modulation superimposed on a spatially periodic Drude medium influences wave dispersion and amplification. Starting from Maxwell's equations and the Drude model, we derive dispersion relations for both homogeneous and periodically modulated systems. The time modulation introduced via synthetic motion is treated using a Galilean transformation to a co-moving frame, subsequently allowing the use of a transfer matrix method and Bloch's theorem to construct the band structure of the space-time crystal. The analysis reveals critical modes at which the system exhibits parametric amplification, a signature of non-Hermitian behaviour and energy exchange between the modulation and the wave. We first examine plane waves which are normally incident to the periodic interfaces, and then generalise them to oblique incidence by introducing TE and TM polarisations. We find that amplification is not confined to paraxial regimes; in some configurations, oblique incidence even enhances gain. To interpret these effects, we use ideas from pertubation theory to obtain approximate analytic expressions for the complex frequency modes responsible for amplification. This research contributes to a formulation that is specifically tailored to the Drude model. This is relevant to real-world materials such as indium tin oxide, which supports optical-range plasma frequencies and is experimentally accessible for realising synthetic motion via ultrafast modulation. Applications of this work include optical isolators, non-reciprocal devices, directional amplifiers, and novel signal processing platforms in both optics and terahertz frequencies. Future directions may include the extension of this framework to quasiperiodic spatial arrangements, which may host richer spectral features and potential for localisation phenomena. This study lays the foundation for engineering tunable, active metamaterials with unprecedented control over light–matter interaction in time and space.

Acknowledgements

Four years at Imperial have passed swiftly. I came into university with an open mind and a passion for science, and I am deeply thankful that this project has allowed me to contribute my tiny piece to the vast puzzle of scientific understanding. While my future may not lie in academia, I have had the privilege of working alongside some of the brightest minds at Imperial. It has been a pleasure to be a part of cutting-edge research at a leading institution.

I owe particular thanks to the *Waves group* led by Richard Craster, where I have benefited from insightful conversations and the opportunity to present my work. I am especially thankful to *Dr Bryn Davies* and *Dr Marc Martí Sabaté*, with whom I worked during my UROP project last summer, which first introduced me to this field. Bryn's guidance was instrumental, particularly as someone from a similar mathematics background, and Marc was a generous mentor, always willing to share his expertise. I also would like to thank *Dr Marie Touboul*, my former undergraduate personal tutor, and another member of this group.

Of course, it would be remiss of me not to pay special tribute to my supervisors: *Professor Richard Craster* and *Dr Raziman Thottungal Valapu*. Richard – it has been an honour to work under your supervision, and I am grateful for your guidance and support and for your invaluable insights shared along the way. Raziman – your mentorship this past year has been amazing, and I thank you for answering my many (often dumb) questions so thoroughly, for guiding me through this project, and for teaching me so much from your perspective, both academic and beyond. Much of what has been achieved in this thesis is a direct result of your constant support.

As I now turn the page to the next chapter of my life, I will deeply miss my time at Imperial. To the *friends* I have made at this university – thank you for the lifelong friendships and unforgettable memories (mostly outside of the classroom, I must confess) that have made my undergraduate years truly special. Finally, I owe my deepest gratitude to my family, whose unwavering love and support has been the backbone of everything I have pursued. In particular, thank you to my *mum*, *dad*, and *sister* for everything.

Contents

List of Figures

Chapter 1

Introduction and State of the Art

1.1 Motivation

The study of electromagnetic (EM) wave propagation in time-varying media has gained substantial traction in recent years, driven by both theoretical curiosity but also by advances in the technology. Among the most compelling material platforms enabling such explorations are *metamaterials*: a type of material engineered to exhibit properties that are not commonly found in nature. Within this class, Drude metamaterials have attracted particular interest due to their plasmonic behaviour - that is, the interaction between light and collective oscillations of free-moving electrical charges in the material - as well as their relatively simple mathematical models that closely mimic how conductive materials like metals respond to electromagnetic fields.

A material of significant experimental relevance in this area is *indium tin oxide* (ITO). ITO behaves like a Drude medium in the optical range and can be engineered to display ultrafast, spatially resolved modulations through optical pumping techniques, [1]. This enables the synthesis of these spatiotemporally varying metamaterials in laboratory settings, and hence the experimental feasibility of such systems provides a strong motivation for theoretical models that accurately describe how EM waves behave in these engineered materials.

Furthermore, the rich physics of time-varying systems, such as parametric amplification and non-reciprocal propagation, offers a pathway to a new generation of photonic devices. Thus, given the prominence and growth of this field, there is both a timely need and practical justification for studying EM wave propagation in time-modulated Drude metamaterials. This thesis contributes to this endeavour by focusing on a Drude space-time crystal (Drude material periodically modulated in both space and time). While prior work has explored similar models using the Drude-Lorentz formulation, [2], this thesis presents a formulation specific to the Drude model, with the hope of near-future experimental realisation using materials like ITO.

1.2 Outline of the thesis

This thesis is organised in the following manner:

- After introducing the foundational theory and situating this work within the broader context of metamaterial research, Chapter 2 begins by examining wave propagation in the case of *normal incidence*. Here, waves encounter the periodic interfaces of the material orthogonally, and the analysis is restricted to variations along a single spatial direction, simplifying the mathematical formulation.
- Once the theoretical and numerical framework for this case is developed, Chapter 3 extends the model to accomodate *obliquely incident waves*. This generalisation involves resolving *transverse electric* (TE) and *transverse magnetic* (TM) polarisations, and adds complexity by introducing an additional spatial wavenumber component.
- In Chapter 4, we employ techniques from *perturbation theory* to develop analytical approximations for the system's critical modes, which helps explain the numerical finding and offers insight into how key parameters influence amplification and stability.
- Chapter 5 concludes the thesis by summarising the key findings and proposing future directions.

1.3 Metamaterials

Metamaterials are artificially structured composite materials that can be engineered to have desirable electromagnetic properties, [3]. Their electromagnetic response arises primarily from their subwavelength structure rather than their chemical composition.

Metamaterials may be characterised by *effective medium parameters*, such as the electric permitivitty ε and the magnetic permitivitty μ, which may attain values not found in naturally occurring materials. This allows for properties such as focusing via negative refraction or spatially varying, anisotropic, refractive index, [4].

By carefully designing the unit cells on a scale much smaller than the wavelength of interest (*i.e.* subwavelength), this allows for control over wave propagation through tailoring of the constitutive relations,

$$\mathbf{D} = \varepsilon_{\text{eff}}\mathbf{E}\,, \quad \mathbf{B} = \mu_{\text{eff}}\mathbf{H}\,. \tag{1.1}$$

Here, $\mathbf{D}$ is the electric displacement field, $\mathbf{E}$ is the electric field, $\mathbf{B}$ is the magnetic field, and $\mathbf{H}$ is the magnetic field intensity. A particularly intriguing class of metamaterials are those with simultaneously negative $\varepsilon_{\text{eff}} < 0$ and $\mu_{\text{eff}} < 0$, giving rise to a negative refractive index.

The underlying principle enabling these effects is the *periodicity* of the metamaterial, which allows the use of *Bloch's theorem* to describe wave propagation.

Bloch's theorem states that: if a material is periodic in space with period p, then the fields $\mathbf{E}$ obey, $\mathbf{E}(r+p) = \mathbf{E}(r)e^{ikp}$, where k is the Bloch wavenumber.

This periodicity gives rise to *photonic band structures*, much like electronic band structures in solids which describe the range of energies that electrons can and cannot occupy in a solid, these show allowed and forbidden frequency ranges for propagation.

1.3.1 Electromagnetic waves in metamaterials

The behaviour of electromagnetic waves in metamaterials is governed by Maxwell's equations (the details and background required for Maxwell's equations is provided in Appendix A.2, and [5] is the main reference for the electromagnetism theory discussed). In source-free regions, Maxwell's equations are

$$\nabla \times \mathbf{E} = -\frac{\partial \mathbf{B}}{\partial t}, \quad \nabla \times \mathbf{H} = -\frac{\partial \mathbf{D}}{\partial t}$$

Using the effective material relations in (1.1) and assuming time-harmonic fields, we can obtain the wave equation in a homogeneous metamaterial,

$$\nabla^2 \mathbf{E} + \omega^2 \varepsilon_{\text{eff}} \mu_{\text{eff}} \mathbf{E} = 0$$

which leads to a dispersion relation of the form $k^2 = \omega^2 \varepsilon_{\text{eff}} \mu_{\text{eff}}$.

Depending on the signs of ε_{eff}, μ_{eff}, the material can support real or imaginary wavevectors k, corresponding to propagating or evanescent modes.

Over the last two decades, research has explored various effects in metamaterial structures, and many of these effects can be dynamically tuned through geometry, external stimuli, or, as in this thesis, *spatiotemporal modulation*.

1.3.2 The field of time-varying metamaterials

A more recent and highly active area of research concerns *time-varying* metamaterials, media whose electromagnetic properties vary dynamically in time, or in both space and time (spatiotemporally). These modulations are typically externally driven, through optical, electrical or acoustic means, enabling ultrafast and reconfigurable photonic systems.

The foundational theoretical work on time-varying media dates back to the 1960s, when Morgenthaler first explored the propagation of electromagnetic waves in materials with time-dependent constitutive parameters [6]. Building on this, later work extended these ideas to space-time periodic structures, culminating in the influential two-part series in [7, 8]. These studies provided the first rigorous mathematical treatment of wave dispersion in periodic space-time media, identifying the formation of band gaps and mode interactions that are now central to modern interpretations of spatiotemporal crystals.

In the decades following, initial interest in time-varying media was found with microwave and acoustic parametric devices. Researchers explored parametric amplifiers for microwaves, where modulating the reactive components of transmission lines enabled frequency conversion and gain, [9, 10]. This set the basis for microwave parametric devices and travelling-wave parametric amplifiers, technologies that remain in radio-frequency and acoustic engineering. The late 1990s to early 2000s marked the start of spatiotemporal photonic crystals as a formal field, driven by progress in microfabrication and inspired by analogies with solid-state physics (concepts of band structures and Brillouin zones). In this period, it was shown that periodically loaded transmission lines could mimic the behaviour of photonic crystals, [11]. In the 2010s there was a growing demand for dynamic photonic components, and the focus shifted to using temporal modulations for achieving non-reciprocal light propagation in photonics. For example, [12] explored how travelling wave modulation could break time-reversal symmetry and lead to unidirectional propagation in photonic systems. At the same time, theoretical frameworks have advanced to include modern treatments of wave propagation in Floquet media, where periodic modulations in time and space are understood through quasi-energy band structures and concepts of parametric amplification, [13, 14, 15].

On the materials side, experimental efforts have likewise made significant breakthroughs. In particular, materials like indium tin oxide (ITO) exhibit Drude-like responses and are compatible with ultrafast optical modulation, [1]. Optical pumping of ITO enables rapid, spatially resolved modulation of its dielectric properties on femtosecond timescales, providing an ideal experimental realisation of time-varying metamaterials, and motivating the theoretical treatment developed in this thesis.

1.3.3 Applications of metamaterials

Metamaterials, and time-varying metamaterials, have broad and impactful applications across various domains. In optics and photonics (as is the focus of this work), they include (adapted mostly from [16]):

- Non-reciprocal devices, such as insolators and circulators, without the need for magnetic biasing. Non-reciprocal devices allow the transmission of waves or signals in one direction but block or restrict the transimission in the opposite direction. They traditionally required magnetic biasing, but now these devices can operate without the need for magnetic fields using time-varying media. [12]

- Compact frequency mixers and converters for on-chip signal processing. Time-varying metamaterials can be engineered to shift the frequency of a signal in a very compact, chip-scale format, which is essential in communication systems. For example, it has recently been used in terahertz generation from near-infrared bands, [17].

- Topological photonics and protected edge states; in certain specially designed metamaterials, light can be made to travel along the boundaries the material in a way that it is immune to defects, so even if the material has imperfections, the light continues

to propagate without scattering. This is a topologically protected mode, and these features are useful for creating robust optical waveguides. [15]

- Parametric amplifiers, which uses energy from a time-varying pump to amplify signal waves, offering low-noise amplification which is very important for sensitive applications like radio astronomy and secure communications. [16]
- Recently, analog optical computing and simulation of complex differential equations; time-varying materials can emulate dynamic processes that mirror the time evolution of analog systems, such as differential equations, enabling direct optical analog simulation in photonic platforms. [18]

Beyond photonics, metmaterials are also used in acoustics, mechanics and thermodynamics, suggesting that the design principles explored in this work could extend to a broader class of wave systems.

1.4 The Drude model

The *Drude model* provides a classical description of the electromagnetic response of conduction electrons in metals and plasmas. We will introduce the Drude model, contrast it with the Drude-Lorentz model, and derive the associated dispersion relation for electromagnetic waves in a Drude medium, adapted from [19].

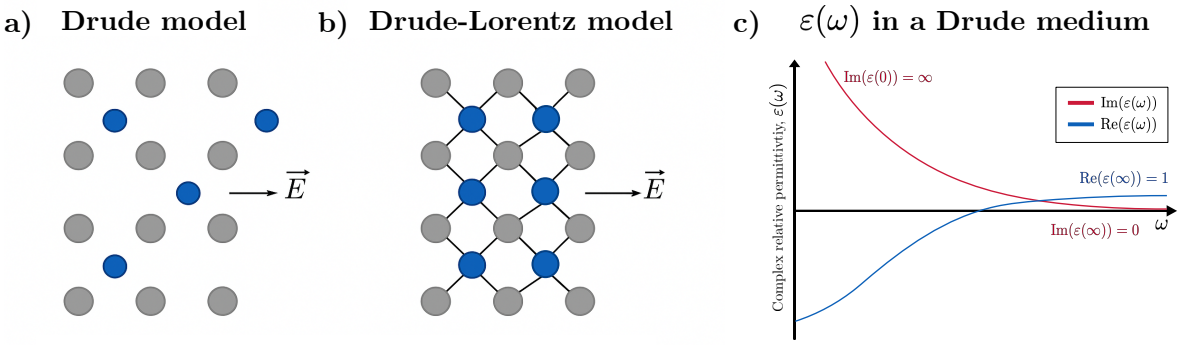

Figure 1.1: **The Drude and Drude-Lorentz models.** a) Schematic of the Drude model, showing free electrons (blue) moving among positive charged ions (grey). b) Schematic of the Drude-Lorentz model, illustrating electrons bound to atomic nuclei by hypothetical. c) Plot of the complex frequency-dependent permittivity $\varepsilon(\omega)$ for the Drude medium, displaying how the material's permittivity varies with the frequency ω of an applied electromagnetic wave. This captures the transition from *metallic* (negative real permittivity) to *dielectric* (positive real permittivity) behaviour.

1.4.1 Comparison with the Drude-Lorentz model

In the Drude model, the conduction electrons are considered to be free particles that respond to external electric fields but experience a damping force due to scattering. The absence of a

restoring force is what distinguishes the Drude model from the Drude-Lorentz model, which includes bound charges oscillating under a restoring potential.

Hence, the oscillation dynamics in the Drude model are an extension of the Drude-Lorentz model to a case where there is zero restoring force. In the Drude model,

$$\ddot{\mathbf{r}} = -\gamma\dot{\mathbf{r}} + \frac{q}{m}\mathbf{E} \tag{1.2}$$

In the Drude-Lorentz model,

$$\ddot{\mathbf{r}} = \omega_0^2\mathbf{r} - \gamma\dot{\mathbf{r}} + \frac{q}{m}\mathbf{E}$$

Here, $\mathbf{r}(t)$ is the displacement of the charge carrier, q and m are the charge and mass of the carrier, respectively, γ is the damping coefficient, and ω_0 is the natural resonance frequency in the Drude-Lorentz model.

The $-\gamma\dot{\mathbf{r}}$ term is a damping term and $\frac{q}{m}\mathbf{E}$ is the acceleration due to the electric force. Note that in the time-varying model, we will have that m is changing and this is the time-varying term.

1.4.2 The Drude dispersion relation

To obtain the frequency-dependent permittivity of a Drude medium, we start by equivalently writing (1.2) as $\dot{\mathbf{v}} = -\gamma\mathbf{v} + \frac{q}{m}\mathbf{E}$, with $\dot{\mathbf{r}} = \mathbf{v}$.

We take our local field $\mathbf{E}$ to vary in time as $e^{-i\omega t}$. In linear systems, the response to a sinusodial driving force will also be sinusodial with the same frequency, hence the response of the electron in the Drude model (*i.e.* its position, velocity) will then oscillate with the same frequency ω.

Therefore, using the behaviour of $\mathbf{v}$ as $e^{-i\omega t}$ and using $\dot{\mathbf{v}} = -\gamma\mathbf{v} + \frac{q}{m}\mathbf{E}$, we obtain

$$\mathbf{v}(\omega) = \mathbf{v}_0 e^{-i\omega t} = \frac{q}{m\left(-i\omega + \gamma\right)}\mathbf{E}$$

Similarly, from the dynamics, we have for $\mathbf{r}$

$$\mathbf{r} = \frac{-q}{m\left(\omega^2 + i\omega\gamma\right)}\mathbf{E}$$

The current density (due to free currents) $\mathbf{J}$ is given by $\mathbf{J} = nq\mathbf{v}$ (where n is the number density of the charges, electrons in this case).

Using Ohm's law for current density, we also have $\mathbf{J}(\omega) = \sigma(\omega)\mathbf{E}(\omega)$, for conductivity σ.

$$\implies \sigma(\omega) = \frac{nq^2}{m(-i\omega + \gamma)}$$

The electric displacement $\mathbf{D}$ can be related to the polarisation $\mathbf{P}$ as $\mathbf{D} = \varepsilon_0\mathbf{E} + \mathbf{P}$. At the

same time, we know in our linear medium $\mathbf{D} = \varepsilon\mathbf{E}$.

$$\implies \mathbf{P} = (\varepsilon - \varepsilon_0)\,\mathbf{E}$$

Assuming non-interacting charges, the polarisation $\mathbf{P}$ can be equivalently written as the charge density multiplied by the polarisation due to a single charge (which is the displacement multiplied by the charge).

$$\implies \mathbf{P}(\omega) = nq\mathbf{r}(\omega) = \frac{-nq^2}{m\left(\omega^2 + i\omega\gamma\right)}\mathbf{E}$$

$$\therefore\ \varepsilon(\omega) = \varepsilon_0 - \frac{nq^2}{m\left(\omega^2 + i\omega\gamma\right)} = \varepsilon_0 - \frac{\sigma(\omega)}{i\omega}$$

Maxwell's equations give the wave equation for the electric field in the medium.

$$\nabla^2\mathbf{E} - \mu_0\varepsilon\frac{\partial^2\mathbf{E}}{\partial t^2} = 0$$

For a plane wave of the form $\mathbf{E} \sim e^{i(\mathbf{k}\cdot\mathbf{r} - \omega t)}$, we obtain the following dispersion relation.

$$\frac{k^2}{\omega^2} = \mu_0\varepsilon(\omega) = \mu_0\left(\varepsilon_0 - \frac{nq^2}{m\left(\omega^2 + i\omega\gamma\right)}\right)$$

We can use the plasma frequency $\omega_p = \sqrt{\frac{nq^2}{m\varepsilon_0}}$.

$$\implies \varepsilon(\omega) = \varepsilon_0\left(1 - \frac{\omega_p^2}{\omega^2 + i\omega\gamma}\right)$$

And the appropriate Drude dispersion relation can be obtained from substituting the expression for $\varepsilon(\omega)$ into $\frac{k^2}{\omega^2}$ above. The graph of $\varepsilon(\omega)$ in Figure 1.1 c) illustrates the behaviour of the complex frequency-dependent permittivity of the Drude medium.

1.5 Synthetic motion

The notion of *synthetic motion* arises in time-varying media, where the electromagnetic properties of a material, typically permittivity ε or permeability μ, are modulated in space and time in a coordinated manner.

While the underlying medium remains stationary in space, the modulation pattern itself propagates like a wave, giving the illusion of motion. As a result, this 'synthetic' motion allows us to explore situations that would otherwise be inaccessible in naturally moving materials, most notably *superluminal motion* (*i.e.* motion faster than the speed of light).

In traditional moving media, actual material motion is limited by mechanical constraints and relativistic effects. However, synthetic motion bypasses these restrictions. Crucially, since the physical constituents of the material remain fixed, no laws of special relativity are violated,

and the modulation carries the synthetic motion, not the medium itself.

[1] provides a clear demonstration of synthetic motion, by modulating the reflectivity of a thin indium tin oxide (ITO) film using ultrafast laser pulses in order to create a moving perturbation in the material's optical properties.

1.5.1 Travelling wave modulation

In this work, for our setup, we focus on a particular type of synthetic motion, a *travelling wave modulation*. This is a modulation of the material parameters that travels as a *periodic wave* in both space and time. If the modulated parameter at some (z, t) is given by $\varepsilon(z, t)$, then with the travelling wave modulation we have

$$\varepsilon(z, t) = \varepsilon(z - vt)$$

where v is the modulation velocity.

Physically, this travelling wave may be thought of as a 'moving background', through which an electromagnetic wave propagates.

Chapter 2

Normally Incident Amplifying Waves in Drude Space-Time Crystals

In this chapter, we study the propagation of plane EM waves normally incident to the periodic interfaces of a Drude space-time crystal. We begin by deriving the governing equations of the system, and non-dimensionalise these to highlight key physical parameters. Focusing on normal incidence, we fix the polarisation to reduce the problem to one varying spatial dimension, and we derive the analytical wave solutions in a homogeneous Drude medium. To extend this to the space-time crystal, we introduce a travelling wave modulation, and move to a co-moving frame where the time modulation appears stationary. Using a transfer matrix approach, we construct the dispersion relation of the crystal and numerically plot its band structure. The chapter concludes with a qualitative analysis of these dispersion profiles under varying system parameters.

Note: The core ideas presented in this chapter were originally proposed by my supervisor, T. V. Raziman; I have rigorously re-derived all results and formulated the presentation and analysis in my own words.

2.1 Governing equations of the system

We begin by formulating the fundamental equations that govern the behaviour of the fields in a Drude medium. These consist of Maxwell's equations in the presence of free currents, as

well as the dynamics of conduction electrons as described by the Drude model.

$$\nabla \times \mathbf{E} = -\mu_0 \frac{\partial \mathbf{H}}{\partial t}$$
$$\nabla \times \mathbf{H} = nq\mathbf{v} + \varepsilon_0 \frac{\partial \mathbf{E}}{\partial t}$$
$$\frac{\mathrm{d}\mathbf{v}}{\mathrm{d}t} = -\gamma \mathbf{v} + \frac{q}{m}\mathbf{E}$$

These follow from our relations $\mathbf{D} = \varepsilon_0 \mathbf{E}$ (ε_0 here a not ε since we are only in the presence of free currents), $\mathbf{B} = \mu_0 \mathbf{H}$ in this instance of the Drude medium.

Here, $\mathbf{v}$ is the velocity field of the charge carriers, q and m denote the charge and mass of the electrons respectively, n is the number density, and γ is the damping rate.

2.1.1 Non-dimensionalisation

To simplify the analysis and reduce the number of parameters, we perform a non-dimensionalisation of the system. We rescale variables using characteristic scales to make the equations dimensionless.

Specifically, we introduce the scalings: $\mathbf{E} = E_0 \mathbf{E}'$, $\mathbf{H} = H_0 \mathbf{H}'$, $\mathbf{v} = v_0 \mathbf{v}'$, $\mathbf{r} = L\mathbf{r}'$, $t = t_0 t'$ (and so $\frac{\partial}{\partial t} = \frac{\partial}{\partial t'}\frac{\partial t'}{\partial t} = \frac{1}{t_0}\frac{\partial}{\partial t'}$).

Using these scalings, the governing equations become The governing equations then transform to

$$\nabla' \times \mathbf{E}' = -\frac{\mu_0 L H_0}{E_0 t_0}\frac{\partial \mathbf{H}'}{\partial t'}$$
$$\nabla' \times \mathbf{H}' = \frac{NLqv_0}{H_0}\mathbf{v}' + \frac{\varepsilon_0 L E_0}{H_0 t_0}\frac{\partial \mathbf{E}'}{\partial t'}$$
$$\frac{\partial \mathbf{v}'}{\partial t'} = -\gamma t_0 \mathbf{v}' + \frac{qE_0 t_0}{mv_0}\mathbf{E}' \ .$$

To simplify coefficients, we impose the following relations

$$\frac{NLqv_0}{H_0} = 1, \quad \frac{\varepsilon_0 L E_0}{H_0 t_0} = 1, \quad \frac{\mu_0 L H_0}{E_0 t_0} = 1 \tag{2.1}$$

and using the second and third equations in (2.1), we obtain

$$t_0 = \sqrt{\mu_0 \varepsilon_0} L$$
$$H_0 = \sqrt{\frac{\varepsilon_0}{\mu_0}} E_0$$

From the first equation in (2.1),

$$v_0 = \frac{H_0}{NLq} = \frac{\varepsilon_0 E_0}{Nqt_0}$$

We also define the *plasma frequency* $\omega_p^2 = \frac{Nq^2}{m_0\varepsilon_0}$, and we choose $t_0 = \frac{1}{\omega_p}$. Therefore, our transformed equations become

$$\begin{aligned} \nabla' \times \mathbf{E}' &= -\frac{\partial \mathbf{H}'}{\partial t'} \\ \nabla' \times \mathbf{H}' &= \mathbf{v}' + \frac{\partial \mathbf{E}'}{\partial t'} \\ \frac{\partial \mathbf{v}'}{\partial t'} &= -\underbrace{\gamma t_0}_{\Gamma}\,\mathbf{v}' + \underbrace{\frac{Nq^2 t_0^2}{m\varepsilon_0}}_{\delta}\,\mathbf{E}' \end{aligned} \tag{2.2}$$

In the third equation above, we further introduce the dimensionless parameters Γ and $\delta = \frac{m_0}{m}$, where $m_0 = \frac{Nq^2 t_0^2}{\varepsilon_0}$.

Note that going forward we will typically drop the 'dashed' notation, *e.g.* $\mathbf{E}$ instead of $\mathbf{E}'$, since we will always use the non-dimensionalised equation from here on now.

2.1.2 Fixing a polarisation for normally incident waves

Suppose we focus on waves that are normally incident to the layered medium. Thus, we assume no variation in the transverse directions (*i.e.* $k_x = k_y = 0$) such that the fields only have ∂_z variation.

This fixes the polarisation as: $\mathbf{E} = E_x = E$, $\mathbf{H} = H_y = H$, $\mathbf{v} = v_x = v$, where originally we had $\mathbf{E} = \begin{pmatrix} E_x & E_y & E_z \end{pmatrix}^T$, and analogously for $\mathbf{H}$ and $\mathbf{v}$.

Using our non-dimensionalised form of the equations (2.2), our governing equations become

$$\begin{aligned} \nabla \times \mathbf{E} = \frac{\partial E}{\partial z} &= -\frac{\partial H}{\partial t} \\ \nabla \times \mathbf{H} = -\frac{\partial H}{\partial z} &= v + \frac{\partial E}{\partial t} \\ \frac{\partial \mathbf{v}}{\partial t} = \frac{\partial v}{\partial t} &= -\Gamma v + \delta E \ . \end{aligned} \tag{2.3}$$

One can show that in a non-time-varying Drude medium, the E, H, and v fields are of the form $\sim e^{i(kz-\omega t)}$. The details for this are in Appendix B.1.

2.2 The Drude model with a travelling wave modulation

We now extend to our modulated Drude medium, where the electron mass parameter m is modulated in both space and time.

2.2.1 Periodic bilayer

We define a *periodic bilayer* structure; that is, at some fixed time, the mass m is represented as a periodic bilayer with spatial period $P = z_1 + z_2$.

$$m(z) = \begin{cases} m_1 & \text{for } 0 \leq z < z_1 \\ m_2 & \text{for } z_1 \leq z < P \end{cases}$$

Further, for the time modulation, we assume that this pattern moves at a constant velocity c (or c can be thought of as how fast the mass parameters are changing), so that $m = m(z - ct)$. This represents a travelling wave modulation.

Since we consider the *mass*, $m(z)$, as a function of z, in the definition above m_1, m_2, z_1, z_2 are dimensional quantities. We find the non-dimensionalised equivalents of m_1, m_2 by scaling by m_0, that of z_1, z_2, P by scaling by z_0, and that of the speed c by scaling by $c_0 = (\mu_0 \varepsilon_0)^{-1/2}$.

However, in (2.4), we will see that, with the non-dimensionalisation, this bilayer function is apparent only in the non-dimensional parameter $\delta = \frac{m_0}{m}$.

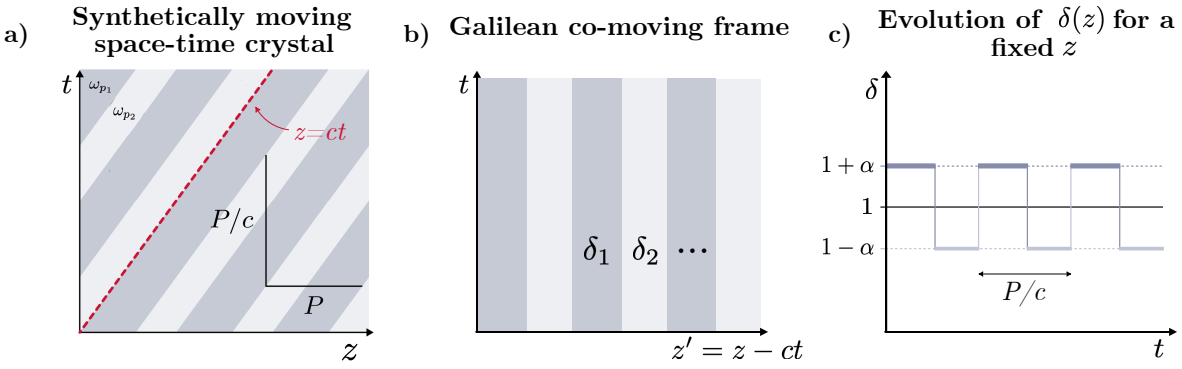

Figure 2.1: **The Drude space-time crystal with synthetic motion.** a) Schematic of the Drude space-time crystal structure shown in a spacetime diagram to display the time-varying property of the material. The Drude metal's plasma frequency is periodically modulated in space and time, alternating between ω_{p_1} and ω_{p_2}, with spatial period P and synthetic motion with speed c. b) Analysis is conducted in a Galilean co-moving frame that transforms the spatiotemporal system into a purely spatial crystal. Each layer is characterised by a dimensionless parameter δ that corresponds to the inverse mass of the charge carriers. c) A graph showing the temporal variation of the parameter δ at a fixed spatial point z within the periodic bilayer crystal. In this structure, δ typically alternates between $1-\alpha$ and $1+\alpha$, where we take 1 as the value of δ in the mean homogeneous medium.

2.2.2 The co-moving frame

To simplify the analysis of this travelling wave modulation, we transform to a co-moving frame. We define coordinates in the co-moving frame as $t_c = t$, $z_c = z - ct$, where z, t are the non-dimensionalised quantities from the governing equations (2.3).

We have the following Jacobian equation for the change of coordinates of the partial derivatives

$$\begin{pmatrix} \frac{\partial}{\partial z} \\ \frac{\partial}{\partial t} \end{pmatrix} = \begin{pmatrix} \frac{\partial z_c}{\partial z} & \frac{\partial t_c}{\partial z} \\ \frac{\partial z_c}{\partial t} & \frac{\partial t_c}{\partial t} \end{pmatrix} \begin{pmatrix} \frac{\partial}{\partial z_c} \\ \frac{\partial}{\partial t_c} \end{pmatrix} = \begin{pmatrix} 1 & 0 \\ -c & 1 \end{pmatrix} \begin{pmatrix} \frac{\partial}{\partial z_c} \\ \frac{\partial}{\partial t_c} \end{pmatrix} .$$

This then gives our *non-dimensionalised*, *transformed* system

$$\begin{aligned} \frac{\partial H}{\partial t_c} &= -\frac{\partial E}{\partial z_c} + c\frac{\partial H}{\partial z_c} \\ \frac{\partial E}{\partial t_c} &= -v + c\frac{\partial E}{\partial z_c} - \frac{\partial H}{\partial z_c} \\ \frac{\partial v}{\partial t_c} &= c\frac{\partial v}{\partial z_c} - \Gamma v + \delta_i E \end{aligned} \tag{2.4}$$

where $\delta_i = \frac{m_0}{m_i}$ for each layer $i \in \{1, 2\}$.

These transformed equations describe the system as seen from a reference frame moving with the modulation.

2.3 Analytical solution in a single layer

To understand wave propagation in each layer of the Drude space-time crystal, we seek *analytical* solutions in the co-moving frame for a single layer $i \in \{1, 2\}$, where the mass m_i would be constant.

We may assume that, in this layer, our fields E_c, H_c, v_c have a dependence of the form $\exp\{i\,(kz_c - \omega t_c)\}$, with amplitudes v_{c0}, E_{c0}, H_{c0}. We can do this since we are in the co-moving frame, and we have shown in Appendix B.1 that the solutions in this case take such a form.

This gives the following equations, substituting the solutions into (2.4).

$$\begin{aligned} kE_{c0} &= (\omega + ck)\, H_{c0} \\ (\omega + ck)\, E_{c0} &= -iv_{c0} + kH_{c0} \\ (\omega + ck + i\Gamma)\, v_{c0} &= i\delta_i E_{c0} \end{aligned}$$

This can be written as the following matrix equation.

$$\begin{pmatrix} -k & \omega + ck & 0 \\ \omega + ck & -k & i \\ -i\delta_i & 0 & \omega + ck + i\Gamma \end{pmatrix} \begin{pmatrix} E_{c0} \\ H_{c0} \\ v_{c0} \end{pmatrix} = 0 \tag{2.5}$$

Non-trivial solutions require the determinant of this matrix to vanish, which gives a *cubic equation* in k. Therefore, in each layer i, there exist three solutions of k corresponding to different modes.

For each layer $i \in \{1, 2\}$, we denote these three solutions for k as k_{ij}, where $j \in \{1, 2, 3\}$, and consequently the electric field amplitudes of the corresponding waves as E_{ij}. The resulting magnetic and velocity field amplitudes can then be obtained from the system (2.5).

$$\begin{aligned} H_{ij} &= \frac{k_{ij}}{\omega + ck_{ij}} E_{ij} \\ v_{ij} &= \frac{i\delta_i}{\omega + ck_{ij} + i\Gamma} E_{ij} \end{aligned} \tag{2.6}$$

2.3.1 Solutions to the homogeneous dispersion relation

Restricting ourselves to one layer and setting $\delta_i = \delta = \frac{m_0}{m}$, then the mode condition results in the determinant of matrix (2.5) being zero.

$$\left(c - c^3\right) k^3 + \left(\omega + i\Gamma - ic^2\Gamma - 3\omega c^2\right) k^2 + \left(\delta c - 3\omega^2 c - 2i\omega c\Gamma\right) k + \left(\delta\omega - \omega^3 - i\omega^2\Gamma\right) = 0$$

Making the substitution $\omega' = \omega + ck$ results in the following 'nicer' cubic equation in ω.

$$\omega'^3 + i\Gamma\omega'^2 - \left(\delta + k^2\right)\omega' - ik^2\Gamma = 0$$

We may make the substitution $\omega' = i\Omega$ (*i.e.* $\omega + ck = i\Omega$), in order to convert our cubic into one with real coefficients (assuming real k).

$$\Omega^3 + \Gamma\Omega^2 + (\delta + k^2)\Omega + k^2\Gamma = 0 \tag{2.7}$$

The cubic discriminant is given by

$$\Delta_3 = \Gamma^2(\delta + k^2)^2 - 4(\delta + k^2)^3 - 4k^2\Gamma^4 - 27k^4\Gamma^2 + 18k^2\Gamma^2(\delta + k^2) \ .$$

Examining the case when k is real, equation (2.7) is a cubic with real coefficients, and hence it must have at least one real solution. Differentiating this cubic gives

$$3\Omega^2 + 2\Gamma\Omega + \delta + k^2 = 2\Omega^2 + (\Omega + \Gamma)^2 + \delta + k^2 - \Gamma > 0 \ .$$

Typically, physically speaking, the parameters of our system satisfy $\Gamma << \delta \sim 1$, and so the derivative above is strictly greater than zero, which implies a strictly increasing cubic. Hence, the other two solutions in this case would be complex conjugates, and thus the cubic has three distinct solutions for Ω.

Of course, a more general condition for obtaining repeated roots would involve finding pairs (Γ, δ) which give real values of k as the solution of the equation $\Delta_3 = 0$. However, this computational exercise is not so important for us, given that we will be in the ranges of $\Gamma << \delta \sim 1$.

2.3.2 Band structure of the homogeneous medium

Before considering the full space-time crystal, we first consider the 'stationary' case, where there is zero *modulation velocity*. The cubic derived in (2.7) describes the band structure within a single homogeneous layer, which we can plot the roots of as in Figure 2.2.

For a periodic bilayer medium, Bloch's theorem allows us to construct the band structure by 'folding' the dispersion relation of the single layer into the Brillouin zone. These folded bands also define frequency intervals where wave can or cannot propagate across the periodic medium (these are also known as *band gaps*).

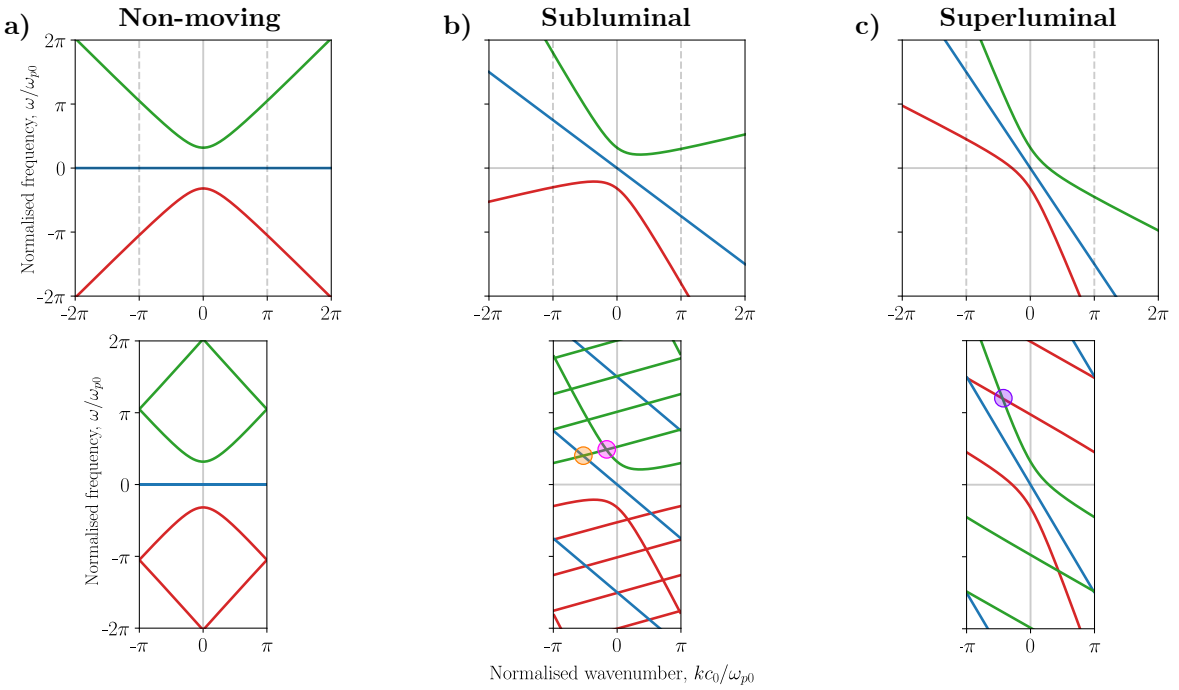

Figure 2.2: **Normal mode crossings in a homogeneous space-time medium.** a) The unmodulated Drude medium's dispersion profile (top plot): two hyperbolic branches of positive frequencies (green) and negative frequencies (red) and a zero-frequency linear branch (blue). The Brillouin zone folding of the branches (bottom plot) show crossings on the edges and centre only within hyperbola branches. b) In a co-moving frame with synthetic motion in the homogeneous medium, the branches shear. For speeds $0 < c < 1$ (shown in $c = 0.75$), crossings between the hyperbolic and linear branches (orange circle) and within each hyperbolic branch (pink circle) are introduced. c) For speeds $c > 1$ (shown is $c = 1.5$), the positive and negative hyperbolas can cross each other (purple circle).

2.4 Boundary conditions in the periodic bilayer medium

We now impose boundary conditions across the interfaces in the periodic bilayer structure in the co-moving frame. In order to determine the field behaviour across the interfaces of this medium, we integrate the system (2.4) across an infinitesimal ϵ-region around the interface.

This gives us the following *continuity conditions*. Starting with the first equation, we obtain

$$\int_{-\delta}^{\delta} \frac{\partial H}{\partial t_c} \mathrm{d}z_c = -\int_{-\delta}^{\delta} \frac{\partial E}{\partial z_c} \mathrm{d}z_c + c \int_{-\delta}^{\delta} \frac{\partial H}{\partial z_c} \mathrm{d}z_c \,.$$

The LHS is zero, since we are assuming the fields have no temporal discontinuities and so the time derivative is bounded. In other words, we can bound the modulus of the LHS as follows.

$$\left| \int_{-\delta}^{\delta} \frac{\partial H}{\partial t_c} \mathrm{d}z_c \right| = \left| \int_{-\delta}^{\delta} \dot{H} \right| \leq \left| \dot{H}_{\max} \right| \cdot 2\delta \to 0$$

The RHS simply becomes

$$0 = -\left(E^+ - E^-\right) + c\left(H^+ - H^-\right) \,,$$

where E^+, E^- are the fields on the right and left of the boundary respectively.

We can do a similar thing for our second equation.

$$\int_{-\delta}^{\delta} \frac{\partial E}{\partial t_c} + v \mathrm{d}z_c = c \int_{-\delta}^{\delta} \frac{\partial E}{\partial z_c} \mathrm{d}z_c - \int_{-\delta}^{\delta} \frac{\partial H}{\partial z_c} \mathrm{d}z_c \implies 0 = c\left(E^+ - E^-\right) - \left(H^+ - H^-\right)$$

where again similarly the LHS is zero, since neither $\dot{E}$ or v can be unbounded. These show that the fields E, H are continuous since $E^+ = E^-$, $H^+ = H^-$, whenever $c \neq 0, \pm 1$.

Finally, the third equation becomes

$$\int_{-\delta}^{\delta} \frac{\partial v}{\partial t_c} + \Gamma v - \delta E \, \mathrm{d}z_c = c \int_{-\delta}^{\delta} \frac{\partial v}{\partial z_c} \mathrm{d}z_c \implies 0 = c\left(v^+ - v^-\right) \,.$$

This shows that v is continuous if $c \neq 0$. Hence, *all three fields* are continuous across the interface, provided $c \neq 0, \pm 1$. On the other hand, if $c = 0$, then v need not be continuous, and the matrix system in (2.5) reduces to solving a quadratic in k instead of a cubic in this case, and hence only two boundary conditions are required to be satisfied.

2.4.1 Matching fields across layers

To apply the boundary conditions, consider our Drude medium in the co-moving frame as below.

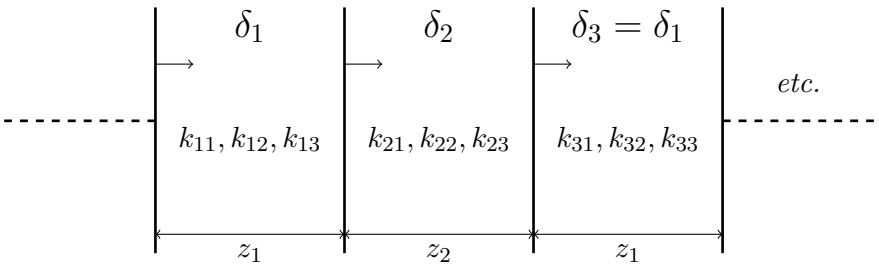

In each layer $i \in \{1, 2\}$, we have three solutions for k, and so we can write the fields as below.

$$\begin{aligned} E_i(\omega; z_c, t_c) &= e^{-i\omega t_c} \sum_{j=1}^{3} E_{ij}(\omega) e^{ik_{ij}(\omega) z_c} \\ H_i(\omega; z_c, t_c) &= e^{-i\omega t_c} \sum_{j=1}^{3} H_{ij}(\omega) e^{ik_{ij}(\omega) z_c} \\ v_i(\omega; z_c, t_c) &= e^{-i\omega t_c} \sum_{j=1}^{3} v_{ij}(\omega) e^{ik_{ij}(\omega) z_c} \end{aligned} \tag{2.8}$$

Note that in the above we are assuming (without loss of generality) that the starting coordinate in each layer is 0. Of course, if we didn't do this then z_c in the equations above would be replaced by $z_c - z_{0i}$ where z_{0i} would be the starting coordinate in layer i.

But, using this approach, the boundary conditions become *matching* the field expressions from layer i and $i+1$ at the interface, some z_k. For example, for the first layer we equate $E_1(\omega; z_1, t) = E_2(\omega; 0, t)$, and the same for H, v.

Substituting the solutions from (2.8) into the boundary conditions and using the results in (2.6), we get the following equations.

$$\begin{aligned} \sum_{j=1}^{3} E_{1j} \exp\left(ik_{1j} z_1\right) &= \sum_{j=1}^{3} E_{2j} \\ \sum_{j=1}^{3} \frac{k_{1j}}{\omega + ck_{1j}} E_{1j} \exp\left(ik_{1j} z_1\right) &= \sum_{j=1}^{3} \frac{k_{2j}}{\omega + ck_{2j}} E_{2j} \\ \sum_{j=1}^{3} \frac{i\delta_1}{\omega + ck_{1j} + i\Gamma} E_{1j} \exp\left(ik_{1j} z_1\right) &= \sum_{j=1}^{3} \frac{i\delta_2}{\omega + ck_{2j} + i\Gamma} E_{2j} \end{aligned}$$

These continuity conditions form the basis for constructing a *transfer matrix system.*

2.4.2 Transfer matrix system

The previous set of equations (2.4.1) can be written in matrix form, defining the amplitude $\Psi_i = \begin{pmatrix} E_{i1} & E_{i2} & E_{i3} \end{pmatrix}^T$.

$$M_{R_1} M_{P_1} \Psi_1 = M_{R_2} \Psi_2$$

Here, we have defined the *region matrix* M_{R_i}, and the *propagation matrix* M_{P_i} as

$$M_{R_i} = \begin{pmatrix} 1 & 1 & 1 \\ \frac{k_{i1}}{\omega + ck_{i1}} & \frac{k_{i2}}{\omega + ck_{i2}} & \frac{k_{i3}}{\omega + ck_{i3}} \\ \frac{i\delta_i}{\omega + ck_{i1} + i\Gamma} & \frac{i\delta_i}{\omega + ck_{i2} + i\Gamma} & \frac{i\delta_i}{\omega + ck_{i3} + i\Gamma} \end{pmatrix}, \; M_{P_i} = \begin{pmatrix} \exp\left(ik_{i1} z_i\right) & 0 & 0 \\ 0 & \exp\left(ik_{i2} z_i\right) & 0 \\ 0 & 0 & \exp\left(ik_{i3} z_i\right) \end{pmatrix}.$$

Similarly, the continuity conditions at the end of the boundary of the second layer can be written as follows.

$$M_{R_2} M_{P_2} \Psi_2 = M_{R_1} \Psi_3$$

But, Ψ_3 is the amplitude of the fields in the third layer, which is a repeat of the first layer due to the spatial periodicity. Hence, by *Bloch's theorem*, we are interested in modes such that $\Psi_3 = e^{i\kappa}\Psi_1$, where $\kappa = \tilde{k}P$ for the period P is the *crystal wavevector*.

$$\implies M_{R_2} M_{P_2} M_{R_2}^{-1} M_{R_1} M_{P_1} \Psi_1 = e^{i\kappa} M_{R_1} \Psi_1$$

To transform this into an eigenvalue problem we make the substitution $\Psi' = M_{R_1}\Psi_1$.

$$\therefore \underbrace{\left(M_{R_2} M_{P_2} M_{R_2}^{-1}\right)}_{\text{call this } M_2} \underbrace{\left(M_{R_1} M_{P_1} M_{R_1}^{-1}\right)}_{\text{call this } M_1} \Psi' = e^{i\kappa}\Psi'$$

We can compute κ by finding the eigenvalues of $M(\omega) = M_2 M_1$, giving us the dispersion relation κ as a function of ω. We obtain 3 solutions for $\kappa(\omega)$ given the 3×3 matrix system.

2.5 Band structure of the Drude space-time crystal

Using the transfer matrix method, we have established that for each *real frequency* ω, the system admits *complex* solutions for the Bloch wavenumber κ, obtained as the eigenvalues of $M(\omega)$. However, it is often more insightful to consider the reverse perspective: to fix *real* values of κ and investigate the resulting *complex* frequencies ω. This approach in particular allows us to identify *amplifying modes*, which are characterised by a positive imaginary component of ω.

To visualise these relationships, we first compute and plot the dispersion profiles for real ω (an example is Figure C.1 a)). Subsequently, to obtain corresponding plots for real κ, we iteratively *track* each branch of $\kappa(\omega)$ back to the real κ-axis by repeatedly making small modifications to ω in the complex plane.

Specifically, we begin by approximating $\frac{\mathrm{d}\kappa}{\mathrm{d}\omega}$ by calculating the wavenumbers at $\omega + \Delta\omega$ (assuming the dispersion relation is analytic), and $\Delta\omega$ chosen small enough to avoid branch mixing. Using this derivative, we take steps in the complex ω plane along a direction that minimises the imaginary part of κ, repeating until $\mathrm{Im}(\kappa)$ falls below a numerical threshold. Once we identify a (ω, κ) pair with real κ, we use the same derivative-based method with $\frac{\mathrm{d}\kappa}{\mathrm{d}\omega}$ to trace the entire branch moving along the real κ line from $-\frac{\pi}{P}$ to $\frac{\pi}{P}$. If the frequencies at $\kappa P = -\pi$ and π differ, we continue into neighbouring branches. By repeating this tracking procedure for all three κ values, using different initial ω guesses, and by discarding any duplicate solutions, we obtain all the branches in the desired frequency range. Plots with complex ω can be seen in Figure 2.3 a) b).

An alternative approach to this tracking method is to consider the function,

$$\min_i \left(|\lambda_i(M_2M_1)| - 1\right)^2$$

which will be zero for each suitable pair (ω, κ), corresponding to a physical mode of the system, where ω would be complex and κ real (here λ means eigenvalue). While this criterion identifies the dispersion relation, it is computationally expensive since it involves searching across every point in an appropriate (ω, κ) grid. Furthermore, this method does not readily preserve the distinctions between the different branches of the dispersion relation. An example of this is shown in the appendix in Figure B.1 c).

2.5.1 Effect of the modulation speed on the extent of amplification

As our intuition would expect, the modulation speed of the synthetic motion directly affects the magnitude of the observed amplification (and it increases with higher modulation speed). For instance, at a modulation speed of $c = 0.7$, shown in Figure B.1 a) b), the normalised imaginary part of the frequency $\mathrm{Im}(\omega)$ reaches only around 10^{-5}, which may be too small to be significant in practical applications. When the speed is reduced further to $c = 0.4$, $\mathrm{Im}(\omega)$ drops to around 10^{-8}, indicating even weaker amplification.

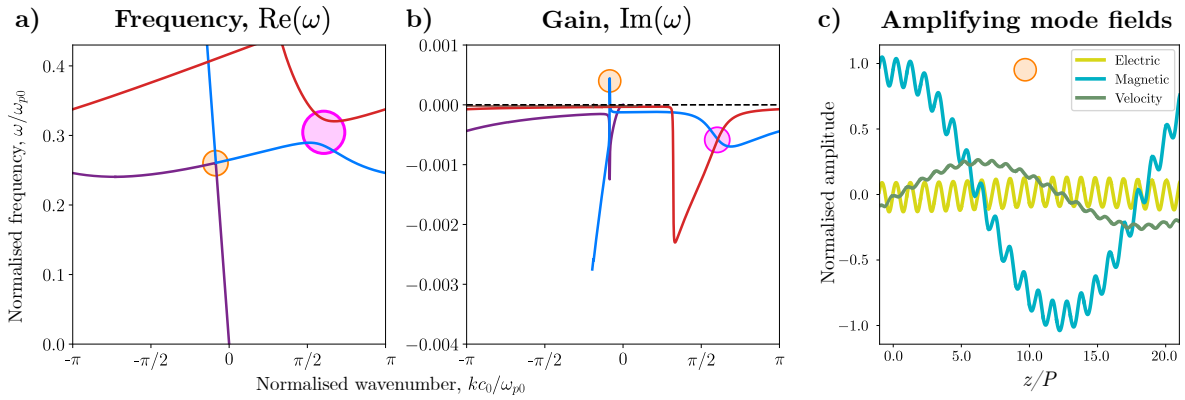

Figure 2.3: **Subluminal amplifying normal waves dispersion in a Drude space-time crystal.** We consider a Drude space-time crystal with parameters $\delta = [1.25, 0.75]$, $\Gamma = 0.01$ and speed of synthetic motion $c = 0.97$. a) Real part of the frequency and b) imaginary parts of the frequency (gain) for admissible modes in the Drude space-time crystal are shown in the dispersion profile. Only the relevant branches are displayed to maintain clarity. The modes arising from the opening of the hyperbola (pink circle) result in a Drude band gap and no amplification. The crossing between the hyperbolic and linear dispersion branches (orange circle) leads to the emergence of a coupled mode that exhibits weak amplification. c) The amplifying mode is shown to be strongly dominated by the magnetic field component, while the electric field contribution remains weak. This dominant magnetic response is attributed to the magnetostatic nature of the linear dispersion branch of the homogeneous medium.

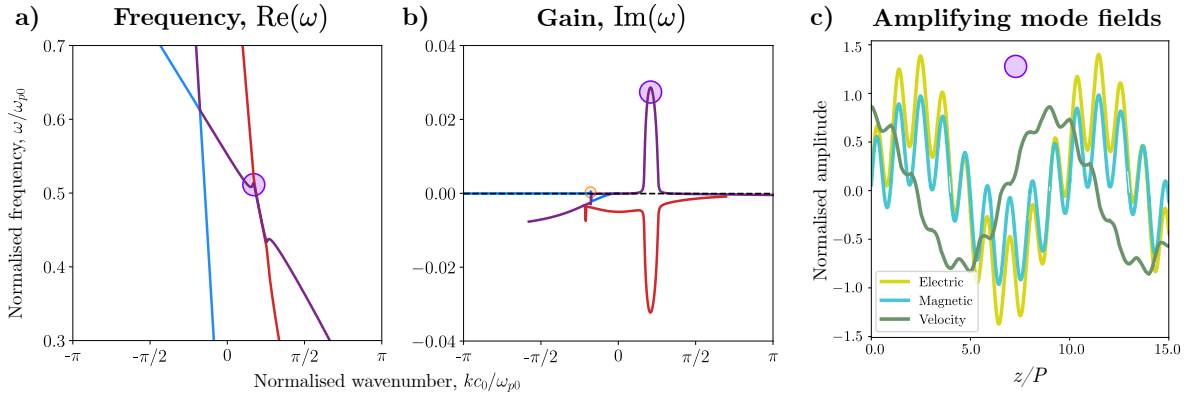

Figure 2.4: **Superluminal amplifying normal waves dispersion in a Drude space-time crystal.** We consider a Drude space-time crystal with parameters $\delta = [1.25, 0.75]$, $\Gamma = 0.01$ and speed of synthetic motion $c = 1.1$. a) Real frequency and b) imaginary gain for modes in the superluminal crystal (only relevant modes are shown). The crossing between the two parabolic branches (purple circle) results in a mode with much higher gain. We also see that the original subluminal amplifying mode remains when the speed is increased to $c > 1$ (orange circle). c) This purple amplifying mode has electric and magnetic field components of similar strengths since it arises from the hyperbolic branch of the homogeneous medium.

2.5.2 The effect of losses in the system

We can vary the parameter Γ, which characterises the losses in our system, and observe how it influences the maximum amplification.

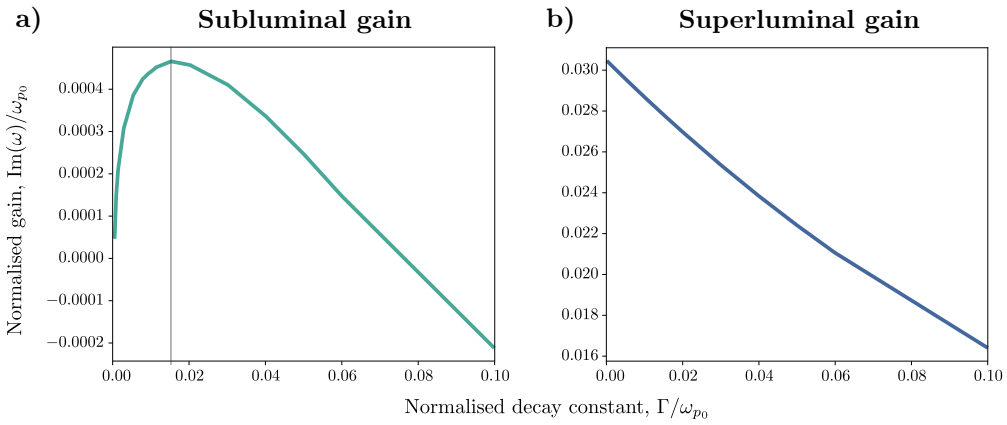

Figure 2.5: **Effect of increasing losses on amplification.** a) Subluminal gain (with $c = 0.97$) where maximum amplification initially increases for small Γ but then diminishes and ultimately vanishes Γ grows beyond a critical value. This indicates an optimal, albeit very small, level of loss for achieving maximum subluminal gain. We can approximate the behaviour of the loss profile as a function of Γ, $\sim \frac{\Gamma(1-0.01\Gamma^2)}{10(\Gamma^2+10)}$; a derivation of this is provided further on in Section 4.2. b) Superluminal gain (with $c = 1.1$) where amplification steadily decreases with increasing Γ, peaking at $\Gamma = 0$ when there are no losses in the medium, which is in line with our intuition.

Chapter 3

Obliquely Incident Amplifying Waves in Drude Space-Time Crystals

In this chapter, we extend the analysis from normally incident waves (Chapter 2) to electromagnetic waves that impinge on the periodic bilayer boundaries of the Drude space-time crystal at *oblique incidence*. This necessitates considering both of the two possible polarisation states: *transverse electric* (TE) and *transverse magnetic* (TM) polarisations. The same overall framework of using Maxwell's equations, the Drude model, the co-moving frame, and the transfer matrix approach is retained, but adapted to the additional spatial dependence introduced by oblique wave propagation.

3.1 TE and TM polarised waves

In Chapter 2, we fixed a polarisation and only considered waves with varying k_z, that is only propagating in the z-direction (also the direction of the temporal modulation). Extending this to the setting of waves that can propagate in both the x- and z- directions now, we have two possible polarisations.

- s- or TE-polarisation: $\mathbf{H} = H_x\hat{\mathbf{i}} + H_z\hat{\mathbf{k}}$, $\mathbf{E} = E_y\hat{\mathbf{j}}$, $\mathbf{v} = v_y\hat{\mathbf{j}}$.
- p- or TM-polarisation: $\mathbf{H} = H_y\hat{\mathbf{j}}$, $\mathbf{E} = E_x\hat{\mathbf{i}} + E_z\hat{\mathbf{k}}$, $\mathbf{v} = v_x\hat{\mathbf{i}} + v_z\hat{\mathbf{k}}$.

In the transverse electric (TE) polarisation, the electric field is oriented entirely in the transverse y-direction, perpendicular to the plane of incidence (the xz-plane). As a result, the magnetic field has components in both the longitudinal and transverse directions. In contrast, in the transverse magnetic (TM) polarisation, the magnetic field is confined to the y-direction, while the electric field lies within the plane of incidence.

The key distinction between TE and TM modes lies in the orientation of the electric field with respect to the plane of incidence; the TE mode has a transverse electric field, while the TM mode has a transverse magnetic field. See [5] for more details on these polarisations.

3.2 Governing equations for the TE system

We first consider the TE-polarisation. Our setup remains the same where we are in a time-modulated periodic bilayer Drude medium, which exhibits synthetic motion in the z-direction. We fix $k_y = 0$ for all waves considered in this section and chapter.

Our non-dimensionalised governing equations in vector form in a single-layer become

$$\nabla \times \mathbf{E} = \begin{pmatrix} -\frac{\partial E_y}{\partial z} \\ 0 \\ \frac{\partial E_y}{\partial x} \end{pmatrix} = \begin{pmatrix} -\frac{\partial H_x}{\partial t} \\ 0 \\ -\frac{\partial H_z}{\partial t} \end{pmatrix} = -\frac{\partial \mathbf{H}}{\partial t}$$

$$\nabla \times \mathbf{H} = \begin{pmatrix} \frac{\partial H_z}{\partial y} \\ \frac{\partial H_x}{\partial z} - \frac{\partial H_z}{\partial x} \\ -\frac{\partial H_x}{\partial y} \end{pmatrix} = \begin{pmatrix} 0 \\ v_y \\ 0 \end{pmatrix} + \begin{pmatrix} 0 \\ \frac{\partial E_y}{\partial t} \\ 0 \end{pmatrix} = \mathbf{v} + \frac{\partial \mathbf{E}}{\partial t}$$

$$\frac{\partial \mathbf{v}}{\partial t} = \begin{pmatrix} 0 \\ \frac{\partial v_y}{\partial t} \\ 0 \end{pmatrix} = \begin{pmatrix} 0 \\ -\Gamma v_y \\ 0 \end{pmatrix} + \begin{pmatrix} 0 \\ \delta E_y \\ 0 \end{pmatrix} = -\Gamma \mathbf{v} + \delta \mathbf{E}$$

This gives rise to the following equations for our non-time-modulated equations in a single-layer.

$$\begin{aligned} \frac{\partial H_x}{\partial z} - \frac{\partial H_z}{\partial x} &= v_y + \frac{\partial E_y}{\partial t} \\ \frac{\partial E_y}{\partial z} &= \frac{\partial H_x}{\partial t} \\ \frac{\partial E_y}{\partial x} &= -\frac{\partial H_z}{\partial t} \\ \frac{\partial v_y}{\partial t} &= -\Gamma v_y + \delta E_y \\ \frac{\partial H_x}{\partial x} &= -\frac{\partial H_z}{\partial z} \end{aligned} \tag{3.1}$$

The fifth equation above comes from Maxwell's divergence equation $\nabla \cdot \mathbf{H} = 0$.

3.2.1 Co-moving frame

Suppose we are now in the desired time-modulated setting. To handle this modulation, as before, we may transform to a co-moving frame, through a Galilean transformation ($z \mapsto$

$z - ct$).

$$\begin{aligned}
\frac{\partial E_y}{\partial t} &= c\frac{\partial E_y}{\partial z} + \frac{\partial H_x}{\partial z} - \frac{\partial H_z}{\partial x} - v_y \\
\frac{\partial H_x}{\partial t} &= c\frac{\partial H_x}{\partial z} + \frac{\partial E_y}{\partial z} \\
\frac{\partial H_z}{\partial t} &= c\frac{\partial H_z}{\partial z} - \frac{\partial E_y}{\partial x} \\
\frac{\partial v_y}{\partial t} &= c\frac{\partial v_y}{\partial z} - \Gamma v_y + \delta E_y
\end{aligned} \tag{3.2}$$

We also have Maxwell's first equation, $\frac{\partial H_x}{\partial x} = -\frac{\partial H_z}{\partial z}$, which remains unchanged.

Assuming the fields have the appropriate dependence $\exp\{i\,(k_x + k_z z - \omega t)\}$ within each single-layer (the precise details for *why* we can do this can be found in Appendix C.2), we can obtain the following TE equations.

$$\begin{aligned}
-\omega E_{y_0} &= ck_z E_{y_0} + k_z H_{x_0} - k_x H_{z_0} + iv_{y_0} \\
-\omega H_{x_0} &= ck_z H_{x_0} + k_z E_{y_0} \\
-\omega H_{z_0} &= ck_z H_{z_0} - k_x E_{y_0} \\
-i\omega v_{y_0} &= ick_z v_{y_0} - \Gamma v_{y_0} + \delta E_{y_0} \\
ik_x H_{x_0} &= -ik_z H_{z_0} \implies H_{z_0} = -\frac{k_x}{k_z} H_{x_0}
\end{aligned} \tag{3.3}$$

The system above (3.3) is actually *over-determined* in the sense that substituting the fifth equation into the third results in exactly the second equation.

By eliminating H_{z_0} through the fifth equation in (3.3), the first, second and fourth equations can be completely written as a 3×3 matrix system.

$$\begin{pmatrix} k_z & \omega + ck_z & 0 \\ \omega + ck_z & k_z + \frac{k_x^2}{k_z} & i \\ -i\delta & 0 & \omega + ck_z + i\Gamma \end{pmatrix} \begin{pmatrix} E_{y_0} \\ H_{x_0} \\ v_{y_0} \end{pmatrix} = 0 \tag{3.4}$$

A more rigorous treatment of reducing the system in such a way is provided in Section 3.2.2.

But, we can sense check the system in (3.4); putting $k_x = 0$ in the above, we can recover the matrix from waves in the case of normal incidence as given in (2.5). The only difference is that we have a k above instead of $-k$ previously, which stems from the fact that in this instance we have swapped x and y which is like changing the direction of z, and hence z changes sign (*i.e.* as both k_z and c are along z, they both flip sign).

Taking the determinant of this matrix and setting equal to zero provides us with a cubic which corresponds to part of the homogeneous dispersion relation for TE modes (we have to be careful however since the dimension reduction from 4×4 to 3×3 may make us lose a solution, hence why this condition is only a *part* of the homogeneous dispersion relation).

Another sense check is that we can use the above equations in (3.3) to derive our original well-known Drude dispersion relation. This derivation is given in Appendix C.1.

3.2.2 Reducing the system from 4×4 to 3×3

Let's consider the case with the 4×4 matrix system, ignoring the fifth equation in (3.3) since the other four equations come directly from our governing equations for the 4 fields.

$$\begin{pmatrix} k_z & \omega + ck_z & 0 & 0 \\ -k_x & 0 & \omega + ck_z & 0 \\ \omega + ck_z & k_z & -k_x & i \\ -i\delta & 0 & 0 & \omega + ck_z + i\Gamma \end{pmatrix} \begin{pmatrix} E_y \\ H_x \\ H_z \\ v_y \end{pmatrix} = 0$$

We can simplify this by first considering a plain Drude material with no time-modulation ($c = 0$) and no spatial periodicity ($\delta = 1$). This yields the following matrix.

$$\begin{pmatrix} k_z & \omega & 0 & 0 \\ -k_x & 0 & \omega & 0 \\ \omega & k_z & -k_x & i \\ -i & 0 & 0 & \omega + i\Gamma \end{pmatrix}$$

The mode condition becomes the determinant of the above matrix being equal to zero as follows.

$$\omega \left(\omega^3 + i\Gamma\omega^2 - \left(k_x^2 + k_z^2 + 1\right)\omega - \left(ik_x^2\Gamma + ik_z^2\Gamma\right)\right) = 0$$

As expected, we see a further fourth solution for ω. In particular, we there is an extra solution of $\omega = 0$ arising in this situation (so two of the four solutions are $\omega = 0$).

The eigenvalue corresponding to this solution is $(0, k_x, k_z, 0)$, and hence this represents a purely magnetostatic mode, which cannot exist (unphysical mode) due to Maxwell's equation $\nabla \cdot \mathbf{H} = 0$.

To explain this further, recall from Maxwell's equations $\nabla \times \mathbf{E} = -\frac{\partial \mathbf{H}}{\partial t}$, and taking the divergence of both sides yields $0 = \nabla \cdot \left(\frac{\partial \mathbf{H}}{\partial t}\right)$, which in our case implies

$$-i\omega\nabla \cdot \mathbf{H} = 0 \implies \omega\nabla \cdot \mathbf{H} = 0 \quad \text{so either } \omega = 0 \text{ or } \nabla \cdot \mathbf{H} = 0$$

But, when $\omega = 0$, $\nabla \cdot \mathbf{H} = 0$ has to be true anyway by Maxwell's divergence equation for the magnetic field.

Of course, this is for the $c = 0$, $\delta = 1$ case which makes the algebra slightly neater, but the same principle applies to the general c, δ case too. We can also do the numerics and see that the plots for the solutions in Figure 3.1 a) b) agree with the analytical theory above.

3.3 Transfer matrices for the TE system

3.3.1 Boundary conditions

Since we have now dealt with the fourth eigenvalue from our 4×4 system, we may reduce this TE-polarisation problem to the 3×3 system in (3.4), as originally proposed.

$$\begin{pmatrix} k_z & -\frac{k_z}{k_x}\omega - c\frac{k_z^2}{k_x} & 0 \\ \omega + ck_z & -k_x - \frac{k_z^2}{k_x} & i \\ -i\delta & 0 & \omega + ck_z + i\Gamma \end{pmatrix} \begin{pmatrix} E_{y_0} \\ H_{z_0} \\ v_{y_0} \end{pmatrix} = 0$$

For our boundary conditions, we look back to our governing equations (3.2) and integrate these equations over a small region $-\epsilon$ to ϵ across the periodic boundary, integrating along the z-direction (the direction of the synthetic motion), which gives us

$$\begin{aligned} c\left(E_y^+ - E_y^-\right) + \left(H_x^+ - H_x^-\right) &= 0 \\ c\left(H_x^+ - H_x^-\right) + \left(E_y^+ - E_y^-\right) &= 0 \\ c\left(H_z^+ - H_z^-\right) &= 0 \\ c\left(v_y^+ - v_y^-\right) &= 0\,. \end{aligned}$$

Provided that $c \neq \pm 1$ or $c \neq 0$, then we have that $E_y^+ = E_y^-$, $H_x^+ = H_x^-$, $H_z^+ = H_z^-$, $v_y^+ = v_y^-$, and hence all four fields are continuous across the boundary.

In each layer i, we have three solutions for (k_x, k_z) (or equivalently ω), since we have disregarded the fourth (k_x, k_z) associated with $\omega = 0$. This allows us to write the fields as follows (in the co-moving frame).

$$\begin{aligned} E_{y_i}(\omega; x_c, z_c, t_c) &= e^{-i\omega t_c} \sum_{j=1}^{3} E_{y_{ij}}(\omega) e^{ik_x(\omega)x_c} e^{ik_{z_{ij}}(\omega)z_c} \\ H_{x_i}(\omega; x_c, z_c, t_c) &= e^{-i\omega t_c} \sum_{j=1}^{3} H_{x_{ij}}(\omega) e^{ik_x(\omega)x_c} e^{ik_{z_{ij}}(\omega)z_c} \\ H_{z_i}(\omega; x_c, z_c, t_c) &= e^{-i\omega t_c} \sum_{j=1}^{3} H_{z_{ij}}(\omega) e^{ik_x(\omega)x_c} e^{ik_{z_{ij}}(\omega)z_c} \\ v_{y_i}(\omega; x_c, z_c, t_c) &= e^{-i\omega t_c} \sum_{j=1}^{3} v_{y_{ij}}(\omega) e^{ik_x(\omega)x_c} e^{ik_{z_{ij}}(\omega)z_c} \end{aligned}$$

For each layer $i \in \{1, 2\}$, we denote the three solutions for $k_{z_{ij}}$ with $j \in \{1, 2, 3\}$. Note that k_x must be the same everywhere across layers due to phase matching and the nature of plane waves. Explicitly, if we have plane wave across an interface with the wave vector k_x parallel to the interface, then the only way to match these is to have $k_{x_1} = k_{x_2}$ to satisfy the continuity condition. Alternatively, we have a linear system which is translationally invariant along x, and so the system must conserve momentum along x.

We also have from (3.3) that the amplitudes of our fields satisfy the following.

$$\begin{aligned} H_{x_{ij}} &= -\frac{k_{z_{ij}}}{\omega + ck_{z_{ij}}} E_{y_{ij}} \\ H_{z_{ij}} &= \frac{k_x}{\omega + ck_{z_{ij}}} E_{y_{ij}} \\ v_{y_{ij}} &= \frac{i\delta_i}{\omega + ck_{z_{ij}} + i\Gamma} E_{y_{ij}} \end{aligned} \tag{3.5}$$

Substituting these results into our boundary conditions (so equating $E_{y_1}(\omega, z_1, t) = E_{y_2}(\omega, 0, t)$, and the same for H_x, H_z, v_y) gives us the final following equations which will help set up our transfer matrices. We equate the E_1 at z_1 with E_2 at 0 *etc.*

$$\begin{aligned} \sum_{j=1}^{3} E_{y_{1j}} \exp\{ik_{z_{1j}} z_1\} &= \sum_{j=1}^{3} E_{y_{2j}} \\ \sum_{j=1}^{3} \frac{k_{z_{1j}}}{\omega + ck_{z_{1j}}} E_{y_{1j}} \exp\{ik_{z_{1j}} z_1\} &= \sum_{j=1}^{3} \frac{k_{z_{2j}}}{\omega + ck_{z_{2j}}} E_{y_{2j}} \\ \sum_{j=1}^{3} \frac{k_x}{\omega + ck_{z_{1j}}} E_{y_{1j}} \exp\{ik_{z_{1j}} z_1\} &= \sum_{j=1}^{3} \frac{k_x}{\omega + ck_{z_{2j}}} E_{y_{2j}} \\ \sum_{j=1}^{3} \frac{i\delta_1}{\omega + ck_{z_{1j}} + i\Gamma} E_{y_{1j}} \exp\{ik_{z_{1j}} z_1\} &= \sum_{j=1}^{3} \frac{i\delta_2}{\omega + ck_{z_{2j}} + i\Gamma} E_{y_{2j}} \end{aligned} \tag{3.6}$$

When we move to the transfer matrix system, we will want to reduce this to a 3×3 transfer matrix system. Thus, we must check whether we can omit one of the equations from the above (3.6). For ease of notation, let $\alpha_{ij} = \frac{\omega + ck_{z_{ij}}}{\exp\{ik_{z_{ij}} z_i\}}$ and so we can write the first three equations above in matrix form.

$$\begin{pmatrix} \omega + ck_{z_{11}} & \omega + ck_{z_{12}} & \omega + ck_{z_{13}} \\ k_{z_{11}} & k_{z_{12}} & k_{z_{13}} \\ 1 & 1 & 1 \end{pmatrix} \begin{pmatrix} E_{11}\alpha_{11} \\ E_{12}\alpha_{12} \\ E_{13}\alpha_{13} \end{pmatrix} = \begin{pmatrix} \omega + ck_{z_{21}} & \omega + ck_{z_{22}} & \omega + ck_{z_{23}} \\ k_{z_{21}} & k_{z_{22}} & k_{z_{23}} \\ 1 & 1 & 1 \end{pmatrix} \begin{pmatrix} E_{21}\alpha_{21} \\ E_{22}\alpha_{22} \\ E_{23}\alpha_{23} \end{pmatrix}$$

From this matrix equation, we can clearly see that the equation from the first row is equal to ω multiplied by the equation in the third row plus c multiplied by the equation in the second row. Hence, we are free to omit one of the first three equations in (3.6) in our transfer matrix.

3.3.2 Transfer matrix system

Similar to how we proceeded with the normal incidence case, we again recognise that our previous set of equations can be written in matrix form, defining the amplitude vector $\Psi_i = \begin{pmatrix} E_{i1} & E_{i2} & E_{i3} \end{pmatrix}^T$.

We also define the region and propagation matrices as M_{R_i} and M_{P_i} respectively.

$$M_{R_i} = \begin{pmatrix} 1 & 1 & 1 \\ \frac{k_x}{\omega + ck_{z_{i1}}} & \frac{k_x}{\omega + ck_{z_{i2}}} & \frac{k_x}{\omega + ck_{z_{i3}}} \\ \frac{i\delta_i}{\omega + ck_{z_{i1}} + i\Gamma} & \frac{i\delta_i}{\omega + ck_{z_{i2}} + i\Gamma} & \frac{i\delta_i}{\omega + ck_{z_{i3}} + i\Gamma} \end{pmatrix}, \; M_{P_i} = \begin{pmatrix} \exp\{ik_{z_{i1}} z_i\} & 0 & 0 \\ 0 & \exp\{ik_{z_{i2}} z_i\} & 0 \\ 0 & 0 & \exp\{ik_{z_{i3}} z_i\} \end{pmatrix}$$

Observe that we could have made our region matrix 4×3, however we have decided to omit the second boundary condition from the set of equations (3.6) in the previous section (the boundary condition which corresponds to H_z because this directly comes from E_y as $H_{z_{ij}} = \frac{k_x}{\omega + ck_{z_{ij}}} E_{y_{ij}}$). This allows us to reduce our system to a 3×3 case.

The boundary conditions at the end of the first layer can then be written as $M_{R_1} M_{P_1} \Psi_1 = M_{R_2} \Psi_2$. Similarly, the boundary conditions at the end of the second layer become $M_{R_2} M_{P_2} \Psi_2 = M_{R_1} \Psi_3$.

But, we employ Bloch's theorem for Ψ_3, which is the amplitude of the fields in third layer which is the same as the first layer due to the periodicity, and hence $\Psi_3 = e^{i\kappa} \Psi_1$ for some κ which we are interested in.

$$\therefore \; M_{R_2} M_{P_2} M_{R_2}^{-1} M_{R_1} M_{P_1} \Psi_1 = e^{i\kappa} M_{R_1} \Psi_1 \implies M_2 M_1 \Psi' = e^{i\kappa} \Psi',$$

where $M_1 = M_{R_1} M_{P_1} M_{R_1}^{-1}$, $M_2 = M_{R_2} M_{P_2} M_{R_2}^{-1}$, $\Psi' = M_{R_1} \Psi_1$. This is an eigenvalue problem, where we compute κ by finding eigenvalues of $M_2 M_1(\omega)$, in order to obtain our dispersion relation.

The numerically generated dispersion profile figures for these TE modes can be found in Section 3.6.

3.4 Governing equations for the TM system

We next consider *TM polarised* (or p-polarised) EM waves, where we fix $k_y = 0$, in our usual time-modulated periodic bilayer Drude medium setup. The approach will be very similar as that of the TE case.

Recall that in the TM case, the fields in consideration are E_x, E_z, H_y, v_x, v_z. Fixing ourselves to a single-layer, we may use our non-dimensionalised governing equations of the system (2.2) to examine what the fields looks like.

$$\begin{aligned}
\frac{\partial H_y}{\partial t} &= \frac{\partial E_z}{\partial x} - \frac{\partial E_x}{\partial z} \\
\frac{\partial H_y}{\partial z} &= -v_x - \frac{\partial E_x}{\partial t} \\
\frac{\partial H_y}{\partial x} &= v_z + \frac{\partial E_z}{\partial t} \\
\frac{\partial v_x}{\partial t} &= -\Gamma v_x + \delta E_x \\
\frac{\partial v_z}{\partial t} &= -\Gamma v_z + \delta E_z
\end{aligned}$$

Again, we may assume fields proportional to $\exp\{i(k_x x + k_z z - \omega t)\}$ (the precise details for why we can do this are in Appendix C.2).

Therefore, transforming our governing equations into a co-moving frame, we can obtain the following matrix system.

$$\begin{pmatrix}
\omega + ck_z & -k_z & k_x & 0 & 0 \\
-k_z & \omega + ck_z & 0 & i & 0 \\
k_x & 0 & \omega + ck_z & 0 & i \\
0 & -i\delta & 0 & \omega + ck_z + i\Gamma & 0 \\
0 & 0 & -i\delta & 0 & \omega + ck_z + i\Gamma
\end{pmatrix}
\begin{pmatrix}
H_{y_0} \\ E_{x_0} \\ E_{z_0} \\ v_{x_0} \\ v_{z_0}
\end{pmatrix} = 0$$

3.4.1 Reducing the system from 5×5 to 3×3

From Maxwell's equations we know that $\nabla \cdot \mathbf{H} = 0 \implies \frac{\partial H_y}{\partial y} = 0$, but this is clear from our setup anyway since $\partial y = 0$.

Instead let's consider our other governing equations, and in particular consider the divergence of these.

$$\nabla \times \mathbf{H} = \mathbf{v} + \frac{\partial \mathbf{E}}{\partial t} \implies 0 = \nabla \cdot (\nabla \times \mathbf{H}) = \nabla \cdot \mathbf{v} - i\omega \nabla \cdot \mathbf{E}$$

where we have used that $\frac{\partial}{\partial t} = -i\omega$ in our case. Similarly,

$$\frac{\partial \mathbf{v}}{\partial t} = -\Gamma \mathbf{v} + \delta \mathbf{E} \implies -i\omega \nabla \cdot \mathbf{v} = -\Gamma \nabla \cdot \mathbf{v} + \delta \nabla \cdot \mathbf{E}$$

Combining these two equations, we obtain

$$\left(\omega^2 + i\Gamma\omega - \delta\right) \nabla \cdot \mathbf{E} = 0 \tag{3.7}$$

or, equivalently, $\left(\omega^2 + i\Gamma\omega - \delta\right) \nabla \cdot \mathbf{v} = 0$.

So, here problems come when ω satisfies the quadratic (since $\nabla \cdot \mathbf{E}$ and $\nabla \cdot \mathbf{v}$ can be made non-zero here), and as we move to the co-moving frame this represents essentially an infinite number of ω which satisfy this condition. So, this needs to be addressed when moving to a 3×3 system for TM-polarisation.

We may look at the reduced system for a plain non-time-modulated Drude medium, where $c = 0$ and $\delta = 1$.

$$\begin{pmatrix} \omega & -k_z & k_x & 0 & 0 \\ -k_z & \omega & 0 & i & 0 \\ k_x & 0 & \omega & 0 & i \\ 0 & -i & 0 & \omega + i\Gamma & 0 \\ 0 & 0 & -i & 0 & \omega + i\Gamma \end{pmatrix} \begin{pmatrix} H_{y_0} \\ E_{x_0} \\ E_{z_0} \\ v_{x_0} \\ v_{z_0} \end{pmatrix} = 0$$

In the further simplified case of $\Gamma = 0$, the mode condition for the determinant of the above matrix being zero yields further solutions of $\omega = 1$, $\omega = -1$ (which arise as expected from the quadratic (3.7)), and the eigenvectors corresponding to these ω are $(0, -ik_x, -ik_z, k_x, k_z)$ and $(0, ik_x, ik_z, k_x, k_z)$ respectively.

We can do the numerics and see that the plots Figure 3.1 c) d) agree with the analytical consideration above.

3.5 Transfer matrices for the TM system

3.5.1 Boundary conditions

As we did in the previous setting, when considering waves with only normal incidence, we again integrate our governing equations in the co-moving frame over a small $-\epsilon$ to ϵ region along z (the direction of propagation of the synthetic motion).

Using the same reasoning in the previous Section 2.4, we obtain

$$\begin{aligned} c\left(H_y^+ - H_y^-\right) - \left(E_x^+ - E_x^-\right) &= 0 \\ c\left(E_x^+ - E_x^-\right) - \left(H_y^+ - H_y^-\right) &= 0 \\ c\left(E_z^+ - E_z^-\right) &= 0 \\ c\left(v_x^+ - v_x^-\right) &= 0 \\ c\left(v_z^+ - v_z^-\right) &= 0\,. \end{aligned}$$

Now, provided that $c \neq \pm 1$ and $c \neq 0$, then we can see that all three fields must be continuous across the interfaces.

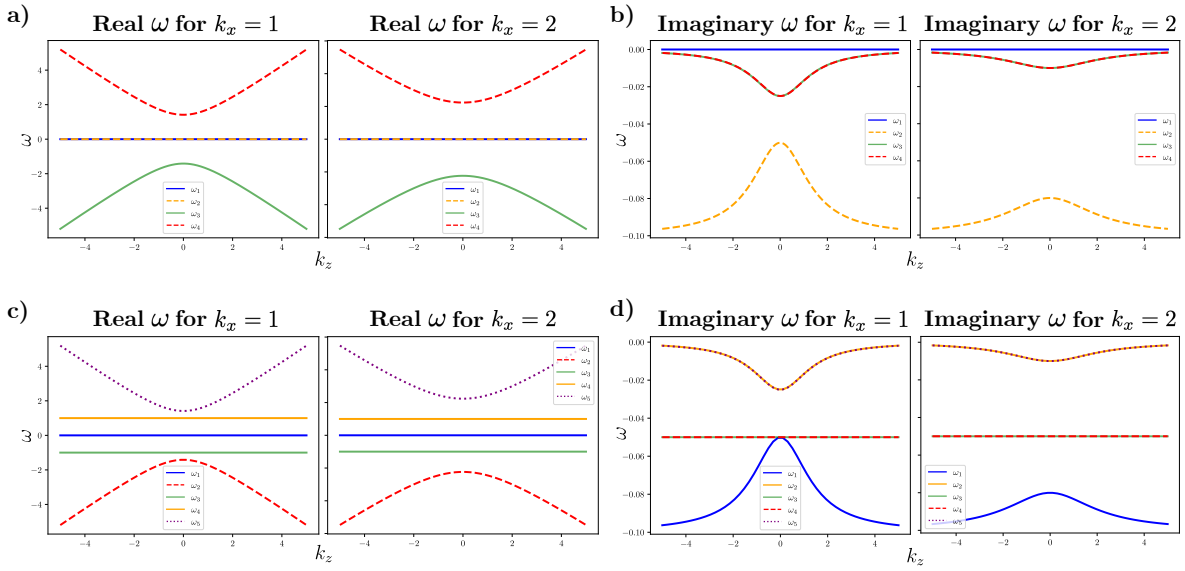

Figure 3.1: **The Drude dispersion solutions for TE and TM waves.** We plot the real and imaginary parts of the complete TE (top) and TM (bottom) dispersion relations of the homogeneous system for two values of k_x, $k_x = 1$ and $k_x = 2$. a) Real parts of the solutions of (k_z, ω) for the TE dispersion relation at $k_x = 1$ (left) and $k_x = 2$ (right). Observe how the gap between the linear branch and hyperbola widens as k_x increases, shifting the crossings within the Brillouin zone. b) Corresponding imaginary parts for the TE dispersion relation at the two values of k_x. c) Real parts of the solutions for the TM dispersion relation at $k_x = 1$ and $k_x = 2$. d) Corresponding imaginary parts for the TM dispersion relation at the two values of k_x. In the same way as in Figure 2.2 b) c), these graphs also become sheared in the presence of synthetic motion and will form analogous branch crossings.

If we want to initially reduce our problem to the 3×3 setting, we have that $\nabla \cdot \mathbf{E} = \nabla \cdot \mathbf{v} = 0$, unless the equation $\omega^2 + i\Gamma\omega - \delta \neq 0$ is satisfied, in which case we *explicitly set* $\nabla \cdot \mathbf{E} = \nabla \cdot \mathbf{v} = 0$. Physically, this means that there can be no charge accumulation at the interfaces. Therefore, our reduced system becomes

$$\begin{pmatrix} \omega + ck_z & k_x & i \\ k_x + \frac{k_z^2}{k_x} & \omega + ck_z & 0 \\ -i\delta & 0 & \omega + ck_z + i\Gamma \end{pmatrix} \begin{pmatrix} E_{z_0} \\ H_{y_0} \\ v_{z_0} \end{pmatrix} = \begin{pmatrix} 0 \\ 0 \\ 0 \end{pmatrix}.$$

As a result, we have that the amplitudes of our three fields being considered satisfy the following equations.

$$\begin{aligned} H_{y_{ij}} &= -\frac{k_x + \frac{k_{z_{ij}}^2}{k_x}}{\omega + ck_{z_{ij}}} E_{z_{ij}} \\ v_{z_{ij}} &= \frac{i\delta_i}{\omega + ck_{z_{ij}} + i\Gamma} E_{z_{ij}} \end{aligned} \tag{3.8}$$

We again equate E_{z_1} at z_1 with E_{z_2} at 0, and the same for H_y, v_z.

$$\sum_{j=1}^{3} E_{z_{1j}} \exp\{ik_{z_{1j}} z_1\} = \sum_{j=1}^{3} E_{z_{2j}}$$
$$\sum_{j=1}^{3} \frac{k_x + \frac{k_{z_{1j}}^2}{k_x}}{\omega + ck_{z_{1j}}} E_{z_{1j}} \exp\{ik_{z_{1j}} z_1\} = \sum_{j=1}^{3} \frac{k_x + \frac{k_{z_{2j}}^2}{k_x}}{\omega + ck_{z_{2j}}} E_{z_{2j}}$$
$$\sum_{j=1}^{3} \frac{i\delta_1}{\omega + ck_{z_{1j}} + i\Gamma} E_{z_{1j}} \exp\{ik_{z_{1j}} z_1\} = \sum_{j=1}^{3} \frac{i\delta_2}{\omega + ck_{z_{2j}} + i\Gamma} E_{z_{2j}}$$

3.5.2 Transfer matrix system

We set up our transfer matrix system with the amplitude vector $\Psi_i = \begin{pmatrix} E_{i1} & E_{i2} & E_{13} \end{pmatrix}$ and we define the following region and propagation matrices.

$$M_{R_i} = \begin{pmatrix} 1 & 1 & 1 \\ \frac{k_x + \frac{k_{z_{i1}}^2}{k_x}}{\omega + ck_{z_{i1}}} & \frac{k_x + \frac{k_{z_{i2}}^2}{k_x}}{\omega + ck_{z_{i2}}} & \frac{k_x + \frac{k_{z_{i3}}^2}{k_x}}{\omega + ck_{z_{i3}}} \\ \frac{i\delta_i}{\omega + ck_{z_{i1}} + i\Gamma} & \frac{i\delta_i}{\omega + ck_{z_{i2}} + i\Gamma} & \frac{i\delta_i}{\omega + ck_{z_{i3}} + i\Gamma} \end{pmatrix}, \quad M_{P_i} = \begin{pmatrix} \exp\{ik_{z_{i1}} z_i\} & 0 & 0 \\ 0 & \exp\{ik_{z_{i2}} z_i\} & 0 \\ 0 & 0 & \exp\{ik_{z_{i3}} z_i\} \end{pmatrix}$$

We do the usual procedure for the transfer matrices. The boundary conditions at the end of the first layer is $M_{R_1} M_{P_1} \Psi_1 = M_{R_2} \Psi_2$, and the boundary conditions at the end of the second layer is $M_{R_2} M_{P_2} \Psi_2 = M_{R_1} \Psi_3$. Bloch's theorem for the periodicity of the system gives $\Psi_3 = e^{i\kappa} \Psi_1$.

$$\therefore \; M_{R_2} M_{P_2} M_{R_2}^{-1} M_{R_1} M_{P_1} \Psi_1 = e^{i\kappa} M_{R_1} \Psi_1 \implies M_2 M_1 \Psi' = e^{i\kappa} \Psi',$$

where $M_1 = M_{R_1} M_{P_1} M_{R_1}^{-1}$, $M_2 = M_{R_2} M_{P_2} M_{R_2}^{-1}$, $\Psi' = M_{R_1} \Psi_1$. We compute κ by finding eigenvalues of $M_2 M_1(\omega)$, in order to obtain our dispersion relation.

3.6 Band structure of the Drude space-time crystal for oblique waves

In our approach, the band structure for TE and TM polarised waves is *identical*. This is because once we reduce the system to 3×3 and disregard the extra solutions arising in Figure 3.1, we can see that we are left with the exact same positive hyperbola branches and the zero-frequency linear branch in both TE and TM. Alternatively, it is not hard to check that they have the same homogeneous cubic, and so they have the same homogeneous band structure when reduced. Moreover, because the transfer matrix approach is the same in both cases, the TE and TM systems will also have the same space-time crystal band structure (*e.g.* Figure 3.2 a) b)). What differs among the two polarisations however is the individual modes. This is evident in the theory, since the mode relations for TE (3.5) are different to that of TM (3.8). For example, the modes are plotted in Figure 3.2 c) d).

3.6.1 Comparison of results between TE and TM polarised waves

We consider the band structures and amplifying modes for TE and TM polarised waves in the subluminal and superluminal regimes.

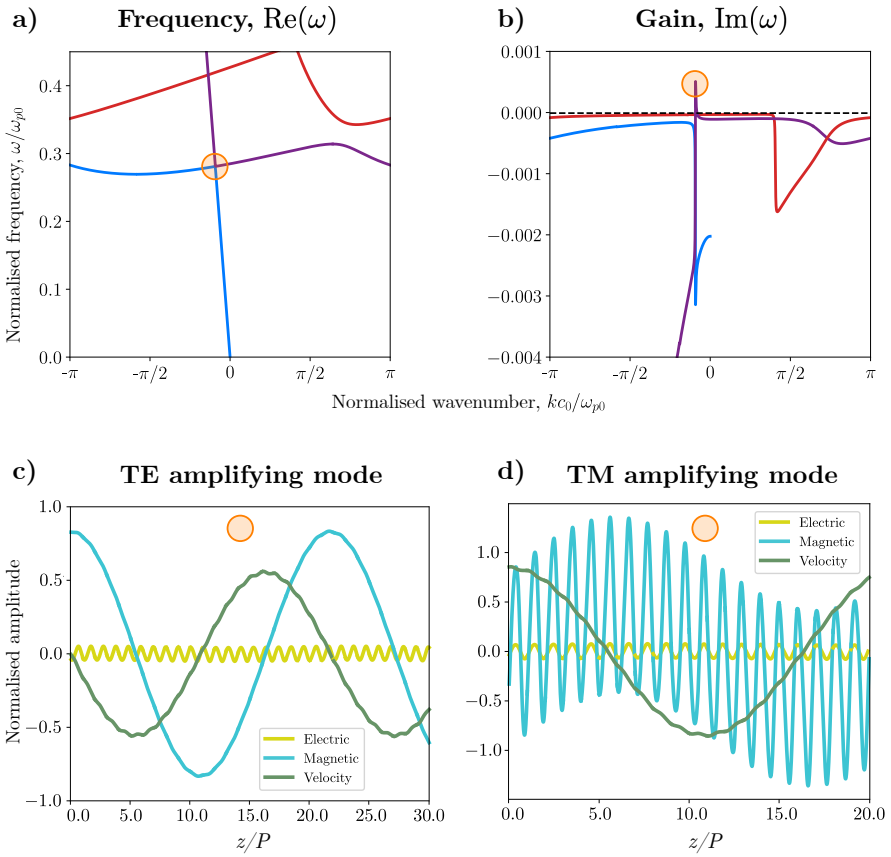

Figure 3.2: **Subluminal amplifying oblique waves dispersion in a Drude space-time crystal.** We consider a Drude space-time crystal with parameters $\delta = [1.25, 0.75]$, $\Gamma = 0.01$, speed of synthetic motion $c = 0.97$, and angle of incidence with $k_x = 0.5$. a), b) The band structure for both TE and TM polarised waves showing real (a) and imaginary (b) parts of the frequency. The crossing shown in the orange circle occurs at a lower wavenumber k_z and higher frequency ω than the corresponding crossing for normal incidence (see Figure 2.3). Subluminal amplification persists even when waves are incident to the material interfaces at angles. In this particular case, the amplification magnitude slightly exceeds that of the normal incidence case, revealing that oblique angles can in fact enhance subluminal gain in certain parameter regimes. c), d) The corresponding field profiles of the amplifying mode for TE (c) and TM (d) polarisations. The TE mode shows a magnetic field dominated structure in quadrature with the velocity field, and the TM mode also exhibits a prominent magnetic field with a much higher frequency; these can be attributed to the magnetostatic nature of the linear dispersion branch of the homogeneous medium.

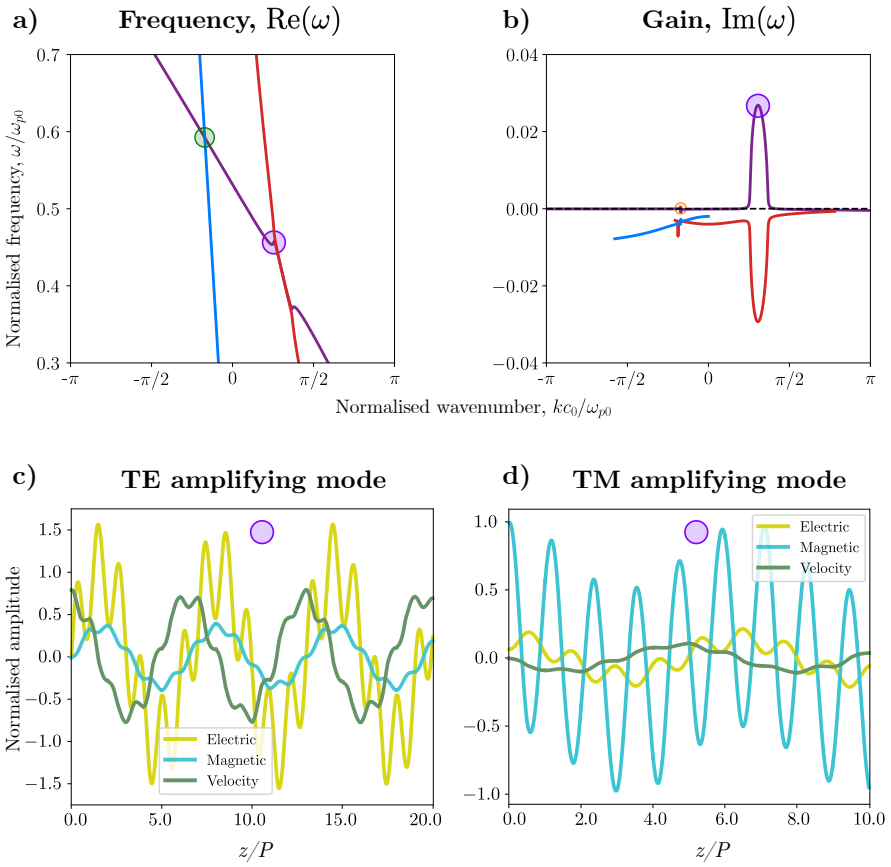

Figure 3.3: **Superluminal amplifying oblique waves dispersion in a Drude space-time crystal.** We consider a Drude space-time crystal with parameters $\delta = [1.25, 0.75]$, $\Gamma = 0.01$, speed of synthetic motion $c = 1.1$, and angle of incidence with $k_x = 0.5$. a) The real part of the frequency ω as a function of κ, showing a distinct crossing (green circle), which in the normal incidence case instead displayed an anti-crossing (see Figure 2.4 a)). This shift from anti-crossing to true crossing signifies that the superluminal motion enables the two branches to intersect without hybridising. b) The imaginary part of the frequency ω, where we see a significant positive imaginary part indicating robust amplification (purple circle). This is the same mode as in the normal incidence case, formed by the crossing of the positive and negative hyperbolas. c), d) The mode profiles of the strongly amplifying mode show the TM mode exhibiting a strong magnetic field response, with the other two field components significantly less, and the TE mode displaying a stronger electric field although it is more balanced with the other field components.

3.6.2 The effect of obliqueness on amplification in the system

We can vary our parameter k_x, which characterises the obliqueness of waves in our system, and observe how it influences the maximum amplification.

In the case of the subluminal gain, increasing the obliqueness initially increasing the maximum gain, but eventually, after some optimum k_x, the maximum gain starts to decrease with increasing angle (in a similar way to how Γ behaved with subluminal gain). We can approximate the behaviour of the loss profile as a function of k_x, $k_x \sim \frac{k_x^2+0.1}{(k_x^2+1)^2\sqrt{k_x^2+10}}$.

In the case of the superluminal gain, increasing the obliqueness decreases the gain, and its behaviour is approximately $\sim \frac{1}{\sqrt{k_x^2+1}}$. These approximations can be found in Section 4.4.

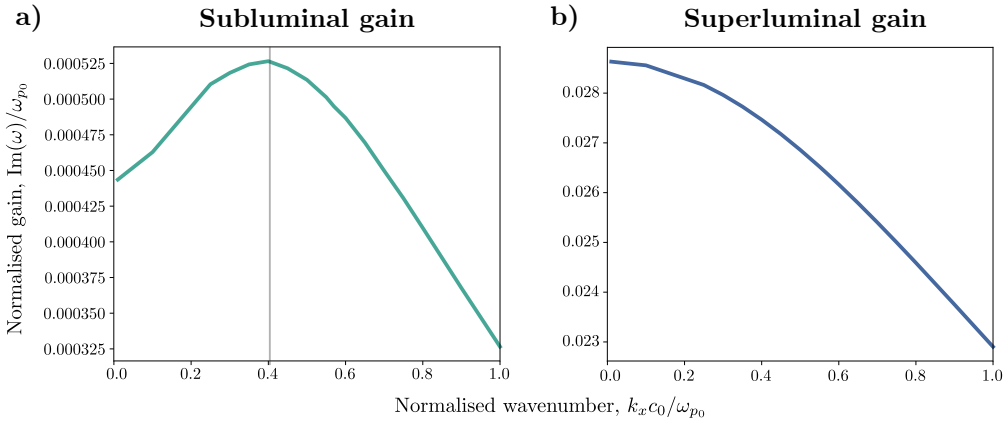

Figure 3.4: **Effect of increasing obliqueness on maximum amplification.** a) Subluminal gain (with $c = 0.97$) showing how small obliqueness actually enhances the extent of amplification up to a certain angle (around $k_x = 0.4$), beyond which it diminishes. b) Superluminal gain (with $c = 1.1$), demonstrating that the strong amplification remains prominent across a broad range of oblique angles, highlighting the robust nature of superluminal gain. However, for this gain, the optimum gain is achieved at normal incidence and any increasing obliqueness diminishes the gain.

Chapter 4

Perturbation Theory to Approximate Critical Modes

In this chapter, we develop an analytical framework to approximate the *critical modes* of the Drude space-time crystal, using techniques from *perturbation theory* and *asymptotic analysis*. Unlike the numerical transfer matrix approach of earlier chapters, this analytical method allows us to understand approximately the system's behaviour without explicit numerics, especially near *branch crossings* where eigenmodes become degenerate or nearly degenerate. The key idea is: away from these branch crossings, the system's modes closely resemble those in a homogeneous Drude medium, but near the crossings, significant phenomena arise, including band gaps and parametric amplification. Hence, we want to be able to develop a scheme to understand analytically the behaviour of modes near to a branch crossing. We adopt a similar mathematical approach to the one done in [2], where they discuss the Drude-Lorentz space-time crystal through the Hamiltonian of the system.

4.1 Perturbation theory mathematical framework for normal incidence

We can think of our bilayer crystal as being composed of a 'mean crystal' plus a perturbation. In this case, the mean crystal is defined with a spatially uniform $\delta = 1$ in every layer. In order to introduce the bilayer periodicity, we add a perturbation α to this mean crystal such that

$$\delta(z) = \begin{cases} 1 + z_2\alpha & \text{if } 0 \leq z < z_1 \\ 1 - z_1\alpha & \text{if } z_1 \leq z < L \end{cases}$$

where $L = z_1 + z_2$ the spatial period. This is a general form for $\delta(z)$ (in order to ensure $\int_0^L \delta(z)\,\mathrm{d}z = L$); instead, in our setup we will take $z_1 = z_2$, and so $\delta(z)$ will look like $1 + \alpha$ for $z \in [0, \frac{L}{2})$, and $1 - \alpha$ for $z \in [\frac{L}{2}, L)$. In our numerical plots, we typically take $\alpha = 0.25$.

The governing equations (2.4) can be recast in the form $M\Psi' + N\Psi = \omega\Psi$, where $\Psi =$

(E, H, v), Ψ' denotes the z-derivative, and we use that $\partial_t = -iw$.

$$M = i\begin{pmatrix} c & -1 & 0 \\ -1 & c & 0 \\ 0 & 0 & c \end{pmatrix}, \quad N = i\begin{pmatrix} 0 & 0 & -1 \\ 0 & 0 & 0 \\ \delta(z) & 0 & -\Gamma \end{pmatrix}$$

We may rewrite this in a more useful form: since Ψ has Bloch periodicity κL, defining $u = \Psi e^{-i\kappa z}$, it is not hard to see that the above matrix equation may be written as

$$Mu' + Pu = \omega u \tag{4.1}$$

where $P = N + i\kappa M$. We also notice that $\delta(z)$ only appears in our P matrix and not M, and so this is the term where our perturbation in the medium comes from. Thus, for the unperturbed or 'mean' system, we may write $M = M_0$, $P = P_0$, and the perturbed system has $M = M_0$, $P = P_0 + \delta P$, where it can be seen that

$$\delta P = \begin{pmatrix} 0 & 0 & 0 \\ 0 & 0 & 0 \\ i(\delta(z) - 1) & 0 & 0 \end{pmatrix}.$$

4.1.1 Defining an inner product

From (4.1), we fix some value of κ and solve the eigenvalue problem to find frequency ω of the perturbed system.

Let u_1, u_2 be the eigenvectors of the unperturbed system with eigenvalues ω_1, ω_2, and suppose the solution under perturbation can be written $u = c_1u_1 + c_2u_2$. This assumption is physically justified because the hybridised modes deviate significantly from the original (unperturbed) modes only in the vicinity of a crossing or near-degenerate point [20]. In these regions, only the two modes closest in frequency strongly interact, while the contributions from other modes are negligible. Consequently, it is enough to consider a two-mode approximation to accurately capture the essential behaviour of the perturbed solutions near these critical crossings.

The perturbed system may be written as:

$$M_0(c_1u_1' + c_2u_2') + (P_0 + \delta P)(c_1u_1 + c_2u_2) = \omega(c_1u_1 + c_2u_1)\,.$$

The unperturbed system may be written as:

$$M_0(c_1u_1' + c_2u_2') + P_0(c_1u_1 + c_2u_2) = \omega_1c_1u_1 + \omega_2c_2u_1\,.$$

Subtracting these two equations yields,

$$\delta P(c_1u_1 + c_2u_2) = \omega(c_1u_1 + c_2u_2) - \omega_1c_1u_1 - \omega_2c_2u_2\,. \tag{4.2}$$

We now introduce the inner product which takes the form

$$\langle \Psi_i, \Psi_j \rangle = \frac{1}{L} \int_0^L E_i^* E_j + H_i^* H_j + v_i^* v_j \, \mathrm{d}z \,,$$

where we want that $\langle \Psi_i, \Psi_j \rangle = \delta_{ij}$ and so we have $|\Psi_i\rangle = C_i \begin{pmatrix} E_i & H_i & v_i \end{pmatrix}$, where C_i is just a normalising factor for Ψ_i.

First considering $\langle \Psi_i | \Psi_i \rangle = 1$, we have

$$\langle \Psi_i | \Psi_i \rangle = 1 \implies \frac{|C_i|^2}{L} \int_0^L |E_i|^2 + |H_i|^2 + |v_i|^2 \, \mathrm{d}z = \frac{|C_i|^2}{L} \int_0^L 1 + \frac{\kappa^2}{|\omega_i'|^2} + \frac{1}{|\omega_i' + i\Gamma|^2} \, \mathrm{d}z = 1$$

$$\therefore \; C_i = \frac{1}{\sqrt{1 + \frac{\kappa^2}{|\omega_i'|^2} + \frac{1}{|\omega_i' + i\Gamma|^2}}}$$

In the above we have taken, without loss of generality, $E = 1$ since it would have been included in the c_i factor anyway and hence cancelled out. Moreover, we are taking the mean delta, $\delta = 1$, and $\omega' = \omega + c\kappa$.

We may also consider $\langle u_i | u_j \rangle$ for when $i \neq j$.

$$\begin{aligned} \langle u_i, u_j \rangle = \langle \Psi_i, \Psi_j \rangle &\propto \int_0^L (E_i^* E_j + H_i^* H_j + v_i^* v_j) \, e^{i(n_j - n_i)\frac{2\pi}{L} z} \, \mathrm{d}z \\ &= (E_i^* E_j + H_i^* H_j + v_i^* v_j) \; L \cdot \delta_{n_i, n_j} \quad = 0 \text{ when } i \neq j \end{aligned}$$

One can show that in the particular case with $\Gamma = 0$, the normalising factor C_i takes a much simpler form, and if additionally $c = 0$, then $C_i = \frac{1}{\sqrt{2}}$. The details for this are provided in Appendix D.1.

4.1.2 Defining the perturbed Hamiltonian to obtain the perturbed frequencies

Using (4.2) and projecting both sides of the equation onto u_1 and u_2, we obtain the following set of equations (using $\langle u_i, u_j \rangle = \delta_{ij}$).

$$\begin{aligned} \langle u_1, \delta P(c_1 u_1 + c_2 u_2) \rangle &= (\omega - \omega_1) c_1 \\ \langle u_2, \delta P(c_1 u_1 + c_2 u_2) \rangle &= (\omega - \omega_2) c_2 \end{aligned}$$

These can be rewritten as follows, defining $\Pi_{ij} = \langle u_i | \delta P | u_j \rangle$.

$$\begin{aligned} (\Pi_{11} + \omega_1) c_1 + \Pi_{12} c_2 &= \omega c_1 \\ \Pi_{21} c_1 + (\Pi_{22} + \omega_2) c_2 &= \omega c_2 \end{aligned}$$

This is equivalent to the matrix equation $H\begin{pmatrix}c_1\\c_2\end{pmatrix} = \omega\begin{pmatrix}c_1\\c_2\end{pmatrix}$ with effective Hamiltonian, $H = \begin{pmatrix}\omega_1+\Pi_{11} & \Pi_{12}\\ \Pi_{21} & \omega_2+\Pi_{22}\end{pmatrix} = \begin{pmatrix}\omega_1 & \Pi_{12}\\ \Pi_{21} & \omega_2\end{pmatrix}$, since we can show that $\Pi_{11}, \Pi_{22} = 0$. Indeed,

$$\begin{aligned}\Pi_{ii} = \langle u_i|\delta P|u_i\rangle &\propto \int_0^L i(\delta(z)-1)v_i^* e^{-in\frac{2\pi}{L}z}e^{i\kappa z}E_i e^{im\frac{2\pi}{L}z}e^{-i\kappa z}\,\mathrm{d}z\\ &= iv_i^*E_i\underbrace{\int_0^L \delta(z)-1\,\mathrm{d}z}_{=0} \;= 0\end{aligned}$$

This integral evaluates to zero, since we are in the case of a symmetric bilayer. We now consider what $\Pi_{ij} = \langle u_i|\delta P|u_j\rangle$ is. We take u_i to be order m and u_j order n.

$$L\langle u_i|\delta P|u_j\rangle = \int_0^L \underbrace{i(\delta(z)-1)}_{\delta P}\underbrace{v_i^* e^{-im\frac{2\pi}{L}z}e^{i\kappa z}}_{u_i}\underbrace{E_j e^{in\frac{2\pi}{L}z}e^{-i\kappa z}}_{u_j}\,\mathrm{d}z$$

Note that Ψ_i, Ψ_j are all basis functions of the unperturbed system and so they may be taken outside of the integral, apart from their exponential spatial components and the $(\delta(z)-1)$ perturbation term.

$$\begin{aligned}\implies L\langle u_i|\delta P|u_j\rangle &= iv_i^*E_j\int_0^L (\delta(z)-1)\,e^{i(n-m)\frac{2\pi}{L}z}\,\mathrm{d}z\\ &= i\alpha v_i^*E_j\underbrace{\left(\int_0^{\frac{L}{2}} e^{i(n-m)\frac{2\pi}{L}z}\,\mathrm{d}z - \int_{\frac{L}{2}}^L e^{i(n-m)\frac{2\pi}{L}z}\,\mathrm{d}z\right)}_{=0,\text{ if } m=n}\\ &= \frac{2\alpha v_i^*E_j}{\frac{2\pi}{L}(n-m)}\left(e^{\pi i(n-m)}-1\right) \qquad \left(=\frac{\alpha L v_i^*E_j}{\pi(n-m)}\left(e^{\pi i(n-m)}-1\right)\right)\end{aligned}$$

We have used that $\delta(z)-1$ equals α for z between 0 and $\frac{L}{2}$ and $-\alpha$ for z between $\frac{L}{2}$ and L in the above. Of course, this integral above being zero only works in our case with the symmetric bilayer.

Observing that $e^{\pi i(n-m)}$ is -1 when $(n-m)$ is odd, and 1 when $(n-m)$ is even, we can rewrite it the expression in a simpler form (assuming $m \neq n$).

$$\langle u_i|\delta P|u_j\rangle = \frac{-2\alpha v_i^*E_j}{\pi(n-m)}\cdot \varnothing_{mn}\,, \quad \text{where } \varnothing_{mn} = \begin{cases}1, & \text{if } n-m \text{ odd}\\ 0, & \text{if } n-m \text{ even}\end{cases} \tag{4.3}$$

But we may take $E_j = 1$ (as this E_j factor would cancel out later anyway) and so $v_i^* = \frac{i}{\omega'^* - i\Gamma}$ (where $\omega' = \omega_i + c\kappa$; ω_i is the relevant ω_1 or ω_2 from the crossing in the mean crystal with which we are concerned).

Near a branch crossing, $\mathrm{Re}(\omega_1) \approx \mathrm{Re}(\omega_2)$. We now know all terms of our matrix H, and so

can find the eigenvalues to determine the perturbed frequency ω.

$$\begin{pmatrix} \omega_1 & \langle u_1|\delta P|u_2\rangle \\ \langle u_2|\delta P|u_1\rangle & \omega_2 \end{pmatrix} \begin{pmatrix} c_1 \\ c_2 \end{pmatrix} = \omega \begin{pmatrix} c_1 \\ c_2 \end{pmatrix}$$

$$\implies \omega = \frac{\omega_1 + \omega_2}{2} \pm \sqrt{\frac{(\omega_1 - \omega_2)^2}{4} + \langle u_1|\delta P|u_2\rangle\langle u_2|\delta P|u_1\rangle}\,, \tag{4.4}$$

where $\langle u_1|\delta P|u_2\rangle\langle u_2|\delta P|u_1\rangle = \frac{-4\alpha^2 v_1^* E_2 v_2^* E_1}{\pi^2(n-m)^2} \cdot \varnothing_{mn} = \frac{-4\alpha^2}{\pi^2(n-m)^2} \left(\frac{i}{\omega_1' + i\Gamma}\right)^* \left(\frac{i}{\omega_2' + i\Gamma}\right)^* \cdot \varnothing_{mn}$.

This expression (4.4) reveals how the modulation-induced coupling leads to mode splitting and, in certain cases, parametric amplification (if $\mathrm{Im}(\omega)$ becomes positive). It provides a physically transparent interpretation of how the interplay between α, ω_1, ω_2, Γ governs amplification and loss in the system. However, we will apply suitable approximations to the terms, in order to determine further simplified equations for the interaction of the various parameters.

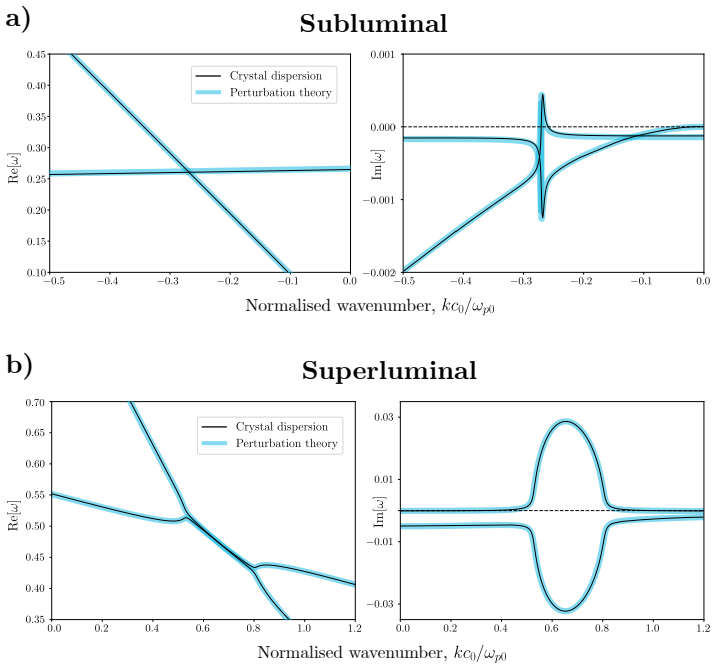

Figure 4.1: **Perturbation theory approximates the amplifying modes.** a), b) Dispersion plots comparing the bands near the amplifying mode obtained from the exact transfer matrix method and the perturbative scheme for subluminal (a) and superluminal (b) systems. The perturbation theory lines closely follow the numerically computed exact values, capturing the main features of the gain profile despite small quantitative deviations.

4.2 Mode approximations and amplification point for normal incidence

The point of amplification occurs when the positive hyperbola branch is folded once in the Brillouin zone and intersects the linear branch at a small value of $\kappa < 0$, as is demonstrated in the orange circle shown in Figure 2.2 b). This is the point we want to focus on for our analysis.

We first obtain approximations for the linear and hyperbola branch, and use these to work out an exact numerical value for the point of intersection. The linear branch can be approximated as

$$\omega_l = -ck_l - i\Gamma\frac{k_l^2}{k_l^2+1}\,,$$

where the 'l' represents linear, and the positive hyperbolic branch can be approximated as

$$\omega_h = -ck_h + \sqrt{k_h^2+1} - \frac{i\Gamma}{2\left(k_h^2+1\right)}$$

where the 'h' represents hyperbolic. Note that k_l, k_h are real and they are not necessarily the same at the amplification point since they only intersect after the folding once in the Brillouin zone. Hence, in fact $k_h = k_l + 2\pi$.

Details on the algebra for where these expressions come from are provided in Appendix D.2.

At the intersection, $k_l \ll 1$ and $k_h \sim 2\pi$ (we can see this from Figure 2.2). To find the point of intersection, k, we can equate the real parts of the frequencies from each branch.

$$-ck = \sqrt{(k+2\pi)^2+1} - c(k+2\pi)$$

Rearranging this gives,

$$4\pi c^2 = (k+2\pi)^2 + 1 \implies k = \sqrt{4\pi^2c^2-1} - 2\pi\,.$$

Substituting $c = 0.97$ into this expression gives the corresponding value for k as $k \approx -0.27$, which matches closely with the value obtained in the numerical plots.

Consider the E, H, z fields for the Ψ_{linear} mode. From (2.6), we have that $H_l = \frac{k_l}{\omega_l + ck_l}E_l$, $v_l = \frac{i\delta}{\omega_l+ck_l+i\Gamma}E_l$. However, we have established that $\omega_l + ck_l = \frac{-i\Gamma k_l^2}{k_l^2+1}$, and so the fields can be written,

$$H_l = \frac{-k_l}{\frac{i\Gamma k_l^2}{k_l^2+1}}E_l = \frac{i(k_l^2+1)}{\Gamma k_l}E_l\,,\quad v_l = \frac{\delta E_l}{\frac{\Gamma}{k_l^2+1}} = \frac{\delta(k_l^2+1)}{\Gamma}E_l\,.$$

From this, we may set $E_l \sim \frac{\Gamma}{k_l^2+1}$, and so $v_l \sim 1$, $H_l \sim \frac{i}{k_l}$ (as $\delta = 1$). We can do this since the actual field value will be taken account for with our normalising factor C_i from the inner product (see Section 4.1.1). Therefore, the normalising factor for this case is

$$C_i = \left(\frac{\Gamma^2}{(k_l^2+1)^2} + \frac{1}{k_l^2} + 1\right)^{-\frac{1}{2}} = \sqrt{\frac{k_l^2}{\Gamma^2 k_l^2 + k_l^2 + 1}}.$$

We do the same thing for our $\Psi_{\text{hyperbolic}}$ mode. We have $H_h = \frac{k_h}{\omega_h + ck_h} E_h$, $v_h = \frac{i\delta}{\omega_h + ck_h + i\Gamma} E_h$, where $\omega_h + ck_h = \sqrt{k_h^2 + 1} - \frac{i\Gamma}{2(k_h^2+1)}$. Setting $E_h \sim 1$ for this case, this gives,

$$H_h \sim \frac{2k_h(k_h^2+1)}{2(k_h^2+1)^{\frac{3}{2}} - i\Gamma}\,, \quad v_h \sim \frac{2i\left(k_h^2+1\right)}{2\left(k_h^2+1\right)^{\frac{3}{2}} + i\Gamma\left(2\left(k_h^2+1\right)-1\right)}\,.$$

The normalising factor in this case is $(1 + H_h H_h^* + v_h v_h^*)^{-\frac{1}{2}} \sim \frac{1}{\sqrt{2}}$ (the details for why this is are provided in Appendix D.3). Now, using (4.4), we care about the *overlap integrals*, $\langle u_1|\delta P|u_2\rangle$ and $\langle u_2|\delta P|u_1\rangle$, since ω_1, ω_2 are known from the point of intersection worked out earlier.

$$\implies P_{lh} = \langle u_l|\delta P|u_h\rangle = \frac{-2\alpha v_l^* E_h}{\pi}\,, \quad P_{hl} = \langle u_h|\delta P|u_l\rangle = \frac{2\alpha v_h^* E_l}{\pi}$$

We derived these formulas earlier (4.3), in the previous section. Note that there is no minus sign in P_{hl} (as opposed to P_{lh}) since the '$n-m$' term from equation (4.3) of the orders of the modes flips from 1 to -1 depending on P_{lh} or P_{hl}.

From these mode approximations, we can obtain the following approximation for $P_{lh}P_{hl}$ (the details of the numerical calculations and algebra have been put in Appendix D.4).

$$P_{lh}P_{hl} \sim \frac{2i\alpha^2}{\pi^2}\frac{\Gamma\left(1 - 0.01\Gamma^2\right)}{10\left(\Gamma^2 + 10\right)} \tag{4.5}$$

4.2.1 Explaining amplification with respect to the losses in the system

To understand amplification in the relevant mode of the crystal, we focus on the *imaginary part* of the perturbed frequency, as this determines both the presence and extent of gain in the system (a larger positive imaginary part implies stronger amplification). From the expression for the perturbed frequency in (4.4), we see that it consists of a central term plus or minus the square root of another term. The central term, depending solely on ω_1 and ω_2, has only a very small negative imaginary part, since there can be no amplification in the unmodulated system.

Thus, it is the term inside the square root that primarily governs whether the overall frequency has a positive imaginary part. Importantly, ω_1 and ω_2 are fixed, so any additional contribution to the imaginary part arises from the product $P_{lh}P_{hl}$, which represents the overlap integrals and their interaction. This product, upon approximation as in (4.5), contains a factor of i multiplying a real-valued expression. Consequently, if the square root of this term acquires a sufficiently large positive imaginary part, selecting the positive sign in the $\pm$ of (4.4) can yield an overall positive imaginary part in the perturbed frequency - signalling amplification.

Therefore, to analyse how the *magnitude* of amplification varies with the damping Γ, it is sufficient to study how the magnitude of $P_{lh}P_{hl}$ (ignoring the i factor) changes. This approach is justified because the square root is a montonically increasing function, and it is not difficult to show that the sign of the imaginary part of $\sqrt{z}$ matches that of the original complex number z. Furthermore, since we only care about the *behaviour* of gain with respect to Γ, we omit any pre-factor terms as well.

$$f(\Gamma) = \frac{\Gamma\left(1 - 0.01\Gamma^2\right)}{10\left(\Gamma^2 + 10\right)} \tag{4.6}$$

Here, the function f approximates the shape of the gain on the perturbed frequency as a function of Γ, using $P_{lh}P_{hl}$. We may plot f and observe how closely it behaves to the numerical profile, Figure 2.5 a).

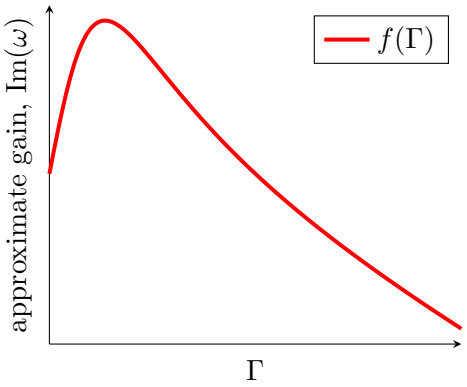

4.3 Perturbation theory mathematical framework for oblique incidence

The setup for the perturbation theory remains the same as we did for the normal incidence case (Section 4.1) when we extend it to oblique waves. Below, we present a treatment for the TE-polarisation case, however the same principles follow for doing it with the TM-polarisation. Moreover, as established in Section 3.6, there is no difference between TE and TM when looking solely at the dispersion profiles of the two for the same system parameters.

As done for the normal incidence case, we want to write our system in the form $M\Psi' + N\Psi = \omega\Psi$. The governing equations of the TE-polarised system are as follows.

$$\begin{aligned}
-i\omega E &= c\frac{\partial E}{\partial z} + \frac{\partial H_x}{\partial z} - ik_x H_z - v \\
-i\omega H_x &= c\frac{\partial H_x}{\partial z} + \frac{\partial E}{\partial z} \\
-i\omega H_z &= c\frac{\partial H_z}{\partial z} - ik_x E \\
-i\omega v &= c\frac{\partial v}{\partial z} - \Gamma v + \delta E
\end{aligned}$$

We may write this in the form $M\Psi' + N\Psi = \omega\Psi$, where

$$M = i\begin{pmatrix} c & 1 & 0 & 0 \\ 1 & c & 0 & 0 \\ 0 & 0 & c & 0 \\ 0 & 0 & 0 & c \end{pmatrix}, \quad N = \begin{pmatrix} 0 & 0 & k_x & -i \\ 0 & 0 & 0 & 0 \\ k_x & 0 & 0 & 0 \\ i\delta & 0 & 0 & -i\Gamma \end{pmatrix}, \quad \Psi = \begin{pmatrix} E \\ H_x \\ H_z \\ v \end{pmatrix}.$$

This can therefore be written in the form of (4.1), where $P = N + i\kappa M$. Again, as before, we have the mean system $M = M_0$, $P = P_0$, and the perturbed system $M = M_0$, $P = P_0 + \delta P$ with δP being the matrix of zeros apart from the bottom left entry which is $i(\delta(z) - 1)$.

We also define a similar inner product (where $\langle u_i, u_j \rangle = \delta_{ij}$),

$$\langle u_i | u_j \rangle = \langle \Psi_i | \Psi_j \rangle \propto \int_0^L \left(E_i^* E_j + H_{x_i}^* H_{x_j} + H_{z_i}^* H_{z_j} + v_i^* v_j \right) e^{i(n_j - n_i)\frac{2\pi}{L}z} \, \mathrm{d}z \, .$$

As a result, the theory in Section 4.1.2 transfers over in the same way, where we can use equation (4.4) to determine the behaviour of the parameters and of the perturbed frequency; the only thing that changes is the individual modes.

4.4 Mode approximations and amplification point for oblique incidence

The mode approximations can be obtained in the same way as done in Appendix D.2 for normal incidence, but instead replacing 'k^2' with '$k_x^2 + k_z^2$' in the ω' expression since the Drude dispersion relation in the oblique case is instead $k_x^2 + k_z^2 = \omega'^2 \left(1 - \frac{1}{\omega'^2 + i\Gamma\omega'}\right)$.

Hence, the linear branch is $\omega_l = -i\Gamma \frac{k_x^2 + k_{z_l}^2}{k_x^2 + k_{z_l}^2 + 1} - ck_{z_l}$, and the hyperbolic branch is $\omega_h = \sqrt{k_x^2 + k_{z_h}^2 + 1} - ck_{z_h} - \frac{i\Gamma}{2\left(k_x^2 + k_{z_h}^2 + 1\right)}$.

For the linear modes, Ψ_{linear}, we have,

$$H_x = \frac{-ik_{z_l}\left(k_x^2 + k_{z_l}^2 + 1\right)}{\Gamma\left(k_x^2 + k_{z_l}^2\right)}E, \quad H_z = \frac{ik_x\left(k_x^2 + k_{z_l}^2 + 1\right)}{\Gamma\left(k_x^2 + k_{z_l}^2\right)}E, \quad v = \frac{\left(k_x^2 + k_{z_l}^2 + 1\right)}{\Gamma}E$$

using (3.5) and since $\omega_l + ck_{z_l} = -i\Gamma \frac{k_x^2 + k_{z_l}^2}{k_x^2 + k_{z_l}^2 + 1}$.

Setting $E \sim \frac{\Gamma}{k_x^2 + k_{z_l}^2 + 1}$, then $H_x \sim \frac{-ik_{z_l}}{k_x^2 + k_{z_l}^2}$, $H_z \sim \frac{ik_x}{k_x^2 + k_{z_l}^2}$, $v \sim 1$. This gives us,

$$\Psi_{\text{linear}} \sim \sqrt{\frac{\left(k_x^2 + k_{z_l}^2\right)}{\left(k_x^2 + k_{z_l}^2 + 1\right)}} \begin{pmatrix} \frac{\Gamma}{k_x^2 + k_{z_l}^2 + 1} \\ \frac{-ik_{z_l}}{k_x^2 + k_{z_l}^2} \\ \frac{ik_x}{k_x^2 + k_{z_l}^2} \\ 1 \end{pmatrix}$$

where the pre-factor is the normalising factor C_i, as before.

We also do the same for the hyperbolic modes $\Psi_{\text{hyperbolic}}$. Using (3.5) and $\omega_h' = \omega_h + ck_{z_h} = \sqrt{k_x^2 + k_{z_h}^2 + 1} - \frac{i\Gamma}{2\left(k_x^2+k_{z_h}^2+1\right)}$, we set $E \sim \omega_h'$, so $H_x \sim -k_{z_h}$, $H_z \sim k_x$, $v \sim i$ (where for v we have taken $\omega' + i\Gamma \approx \omega'$ since Γ is small).

$$\therefore \quad \Psi_{\text{hyperbolic}} \sim \frac{1}{\sqrt{2\left(k_x^2 + k_{z_h}^2 + 1\right)}} \begin{pmatrix} \sqrt{k_x^2 + k_{z_h}^2 + 1} - \frac{i\Gamma}{2\left(k_x^2+k_{z_h}^2+1\right)} \\ -k_{z_h} \\ k_x \\ i \end{pmatrix}$$

It is left to evaluate the overlap integrals $P_{lh} = \langle u_l | \delta P | u_h \rangle$, $P_{hl} = \langle u_h | \delta P | u_l \rangle$. We want to be able to explain any gain in the perturbed frequency, through varying the parameter k_x (*i.e.* the obliqueness). Thus, we care about the imaginary part of the perturbed frequency, and in particular the *positive* contribution to the imaginary part of the perturbed frequency (since ω_1, ω_2 which are from the mean crystal will have very small, negative imaginary part as there can be no amplification in the mean system). From (4.4), the perturbed frequency is given by,

$$\omega = \frac{\omega_1 + \omega_2}{2} \pm \sqrt{\frac{(\omega_1 - \omega_2)^2}{4} + P_{lh} \cdot P_{hl}}\,.$$

Examining this expression, we are at a branch crossing so $\text{Re}(\omega_1) \approx \text{Re}(\omega_2)$, so $(\omega_1 - \omega_2)^2$ will be small, and in particular any additional positive imaginary part will come from $\sqrt{P_{lh}P_{hl}}$. We will approximate P_{lh}, P_{hl}.

$$\begin{aligned} P_{lh} = \langle u_l | \delta P | u_h \rangle &= \frac{1}{L} \int_0^L i\left(\delta(z) - 1\right) v_l^* E_h e^{i\frac{2\pi}{L}z}\, \mathrm{d}z \\ &= \sqrt{\frac{k_x^2 + k_{z_l}^2}{2L^2\left(k_x^2 + k_{z_l}^2 + 1\right)}} \int_0^L i\left(\delta(z) - 1\right) e^{i\frac{2\pi}{L}z}\, \mathrm{d}z \end{aligned}$$

We have taken the imaginary part of E_h as negligible in obtaining the above, since it is a small term and it makes our overall approximations simpler. Recalling that the function $\delta(z) - 1$ is α between 0 and $\frac{L}{2}$, and $-\alpha$ between $\frac{L}{2}$ and L, our integral above evaluates to $\frac{-2\alpha L}{\pi}$.

$$\implies P_{lh} = -\sqrt{\frac{2\left(k_x^2 + k_{z_l}^2\right)}{k_x^2 + k_{z_l}^2 + 1}} \cdot \frac{\alpha}{\pi}$$

Doing the same for P_{hl}, one can obtain

$$P_{hl} = \underbrace{\frac{-i}{\sqrt{2\left(k_x^2 + k_{z_h}^2 + 1\right)}}}_{v_h^*} \cdot \underbrace{\sqrt{\frac{k_x^2 + k_{z_l}^2}{k_x^2 + k_{z_l}^2 + 1}} \frac{\Gamma}{k_x^2 + k_{z_l}^2 + 1}}_{E_l} \cdot \underbrace{\left(\frac{2\alpha}{\pi}\right)}_{\frac{1}{L}\int_0^L i(\delta(z)-1)e^{-i\frac{2\pi}{L}z}\,\mathrm{d}z}$$

$$\therefore \quad P_{lh}P_{hl} = \frac{2i\alpha^2\Gamma}{\pi^2} \frac{\left(k_x^2 + k_{z_l}^2\right)}{\left(k_x^2 + k_{z_l}^2 + 1\right)^2} \frac{1}{\sqrt{k_x^2 + k_{z_h}^2 + 1}} \tag{4.7}$$

We observe that every term in this expression is real except for the factor of i. Therefore, when we take the square root of $P_{lh}P_{hl}$, the presence of $\sqrt{i}$ necessarily introduces a positive imaginary contribution. Consequently, any additional positive imaginary contribution in $\sqrt{P_{lh}P_{hl}}$ must arise from the variation of the real-valued terms in $P_{lh}P_{hl}$ itself (see the beginning of Section 4.2.1 for detailed reasoning). This observation allows us to analyse approximately how the system's amplification varies with k_x at subluminal modulations.

4.4.1 Explaining subluminal amplification with respect to obliqueness

We may plot the behaviour of the expression in (4.7) for varying k_x, and we notice that the behaviour is extremely similar to that of Figure 3.4 a), where we considered numerically the effect of gain on varying parameter k_x at subluminal modulation $c = 0.97$.

For the system under our consideration, we have parameters $\alpha = 0.25$, $\Gamma = 0.01$, $k_{z_l} \approx -0.25$ (at the branch crossing), $k_{z_h} \approx 2\pi - 0.25$. Strictly speaking, the crossing point is also a function of k_x, but it does not vary much as we alter k_x, hence we have kept it constant here for approximation purposes. Therefore, the expression of concern can be written as,

$$f(k_x) = \frac{1.3\text{e}{-4}\left(k_x^2 + 0.06\right)}{\left(k_x^2 + 1.06\right)^2 \sqrt{k_x^2 + 37}} \sim \frac{k_x^2 + 0.1}{\left(k_x^2 + 1\right)^2 \sqrt{k_x^2 + 10}}\,, \tag{4.8}$$

where in the last approximation above we have omitted any constant pre-factors, since we concern ourselves only with the shape. We plot this function below.

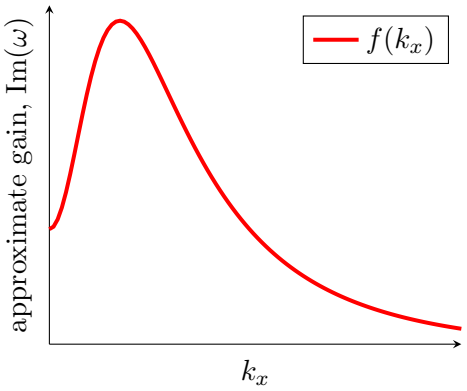

Note that c does not enter explicitly into our analytical approximation (4.7), but is instead included implicitly through approximating $\omega + ck$ of the branches. As a result, there will be certain values of c for which the variation of k_x produces the same profile in our analytical expression, even though the actual magnitude of amplification will be much less. To keep track of this magnitude, one can either make less approximations (in which case the algebra can become very messy), or simply rely on the numerics to give the value of the gain. For instance, for a system with $c = 0.97$, incident waves with $k_x \approx 0.4$ produces the maximum level of amplification.

4.4.2 Explaining superluminal amplification with respect to obliqueness

For superluminal amplification, the branch crossing occurs at a different point. Specifically, it occurs when the negative hyperbola folds in the line $k = -\pi$ and intersects the positive hyperbola in the Brillouin zone.

The branch approximations here for ω_p and ω_n are as follows ('p' denoting from the positive hyperbola branch and 'n' denoting the negative hyperbola).

$$\omega_p \sim \sqrt{k_x^2 + k_{z_p}^2 + 1} - ck_{z_p} - \frac{i\Gamma}{2\left(k_x^2 + k_{z_p}^2 + 1\right)}$$
$$\omega_n \sim -\sqrt{k_x^2 + k_{z_n}^2 + 1} - ck_{z_n} - \frac{i\Gamma}{2\left(k_x^2 + k_{z_n}^2 + 1\right)}$$

Equating these and taking $k_x = 0$, $c = 0$, as an example, the point of intersection occurs when $\sqrt{k_z^2 + 1} + \sqrt{(k - 2\pi)^2 + 1} = 2\pi c$, which can be solved to give $k_z \approx 0.66$. Hence, superluminal amplification for normal incidence occurs at around $k_z = 0.66$, as shown in Figure 2.4 b).

We now deal with the mode approximations. We can work out Ψ_{positive} and Ψ_{negative}, in the same way as done before, and derive an expression for the behaviour as a function of k_x; the details of this have been left in Appendix D.5.

The behaviour of the maximum superluminal gain as a function of k_x can be approximated as,

$$f(k_x) \sim \frac{1}{\sqrt{k_x^2 + 1}}\,.$$

Clearly, this is maximum when $k_x = 0$ (can also be seen in Figure 3.4 b)) and this is a decreasing function for $k_x > 0$, thus this demonstrates that the superluminal amplification is maximised at normal incidence and gradually decays as the angle of incidence is increased.

Summary and outlook of this chapter

We have used the perturbation theory framework to derive analytical insights for the *amplifying modes* of our Drude space-time crystal, as has been the focus in this project. However, one can use the perturbative methods in this same framework to understand a wide range of other features seen in the numerical dispersion profiles - particularly those near branch crossings, where the periodic modulation induces significant deviations from the homogeneous medium behaviour. Ultimately, this analytical framework offers a versatile method for investigating and interpreting a broad spectrum of behaviours in spatiotemporally modulated media, highlighting the power of perturbative analysis in these systems.

Chapter 5

Conclusion and Discussion

Our work has illuminated several key aspects of electromagnetic wave propagating in Drude space-time crystals. We have shown how synthetic motion in these systems, induced by travelling wave modulations, can lead to amplification, but also that amplification is not solely determined by the modulation speed, and the intrinsic properties of the medium and the exact type of incident wave also have an influence on it (in Chapter 2 and Chapter 3). We have also seen that the behaviour of amplifying modes depends critically on whether the modulation is subluminal or superluminal. The perturbative framework developed in Chapter 4 has proven to be a powerful tool for interpreting the numerical findings through an analytical lens. Taken together, these findings demonstrate how Drude space-time crystals can be tailored for dynamic control of electromagnetic waves. While this thesis has focused on the case of periodic bilayer modulations, it sets the foundation for further expansions into more complex geometries as discussed in Section 5.2.

5.1 Summary of key findings

At a very high level, we have found the following in the Drude space-time crystal:

- In certain configurations of the system (*e.g.* symmetric bilayer with $\delta = [1.25, 0.75]$, $c = 0.97$, $\Gamma = 0.01$) we observe parametric amplification. Increasing the modulation to superluminal speeds $c > 1$, new amplifying modes are introduced with much greater amplification.

- For subluminal regimes, increasing the losses of the system Γ initially increases the maximum extent of amplification before decreasing after a small optimal value for Γ. For superluminal regimes, the maximum extent of amplification decreases with increasing Γ.

- For subluminal regimes, increasing the obliqueness of incident waves k_x initially increases the maximum extent of amplification before decreasing after a small optimal value for k_x. For superluminal regimes, the maximum extent of amplification decreases

with increasing k_x.

- When the obliqueness k_x becomes very large beyond a certain point, amplification in the subluminal setting typically vanishes. However, in some superluminal settings, the amplification remains robust and persists for even very high values of k_x.

5.1.1 Parametric amplification in Drude space-time crystals

We can offer an explanation as to why there is a 'sweet spot' in the obliqueness of the wave with respect to the interfaces, where, perhaps counter-intuitively, waves at normal incidence to the interfaces do not always lead to maximum gain.

The amplification observed in space-time crystals arises due to a *parametric interaction* between the travelling-wave modulation and the electromagnetic waves. This interaction is governed by *phase matching conditions*; for amplification to be efficient, the wavevector and frequency of the signal must 'line up' with those of the modulation in a way that allows energy transfer from the modulation to the wave.

As k_x is increased, the wavevector decomposes into both longitudinal and transverse components. At some finite k_x, the transverse and longitudinal components become better 'tuned' to the travelling-wave modulation. Physically, this means that the projection of the wavevector in the direction of the modulation becomes optimal for energy transfer. This is similar to how certain angles of incidence in nonlinear optics maximise frequency mixing processes (such as parametric amplification in crystals), as in [21]. Further details of phase-matching are also provided in [21].

However, the maximum gain at superluminal modulations no longer occurs from the intersection of the folded positive hyperbola and linear branch; instead, it emerges when the positive and negative hyperbola cross. In the superluminal regime, amplification is greatest at $k_x = 0$, *i.e.* normally incident waves, indicating that the phase matching conditions are most favourably aligned in this configuration.

5.2 Future directions

We discuss some potential, useful areas of direction that the work in this project can be extended to, in order to generate additional new physical insights about EM wave propagation in spatiotemporal Drude metamaterials.

5.2.1 Non-symmetric bilayer

The code written as a part of this work, as well as a lot of the theory, generalises to settings where each layer of the bilayer is not of equal length. However, in this project, we have made the convenient choice of focusing specifically on the *symmetric bilayer*, not least because it allows for some of the perturbation theory approximations to fall out nicer than they otherwise would. An interesting direction may be to explore whether there are any significant changes in the system should we alter the lengths of the layers, *i.e.* changing z_1 and z_2.

5.2.2 Allowing for charge accumulation at boundaries

This idea of delving into more detail about charge accumulation is specifically for TM polarised oblique waves. Recall, from the beginning of Section 3.5.1, when reducing the TM system from 5×5 to 3×3, we had to explicitly set $\nabla \cdot \mathbf{E} = \nabla \cdot \mathbf{v} = 0$ whenever ω satisfied $\omega^2 + i\Gamma\omega - \delta = 0$. From Maxwell's equation $\nabla \cdot \mathbf{E} = \frac{\rho}{\varepsilon_0}$, where ρ is the charge density, so in a region with no charge accumulation this quantity is zero.

However, physically, there is no fundamental reason to prohibit charge accumulation at material interfaces or abrupt transitions in material parameters. Such accumulations could manifest as *surface charges* [22] that modify the boundary conditions and potentially give rise to additional interface-bound modes, or altered reflection or transmission properties. To fully capture these effects, one would need to retain the complete 5×5 formulation, especially accounting for electric field components and electron velocities that contribute to $\nabla \cdot \mathbf{E} \neq 0$, $\nabla \cdot \mathbf{v} \neq 0$.

5.2.3 Extension to quasiperiodic media

Instead of the spatially periodic bilayer (period 2) structure explored in this work, one can consider more general geometries such as *quasiperiodic media*, which are known to exhibit rich and exotic wave phenomena. These structures can often be approximated by increasingly large periodic unit cells that converge to a quasiperiodic limit.

A well-known class of one-dimensional quasiperiodic structures is the *Fibonacci tilings*, [23]. These structures are known to support fractal-like band structures and non-trivial spectral gaps. The simplest such sequence is governed by the rule $A \to AB$, $B \to A$. For instance, the length-5 sequence $ABAAB$ provides a quasiperiodic approximant that can replace the symmetric bilayer used here. In this scenario, the parameter $\delta(z)$ would repeat according to the pattern $ABAAB$, so that in layer 'A' we set $\delta(z) = 1 + \alpha$, and in layer 'B' $\delta(z) = 1 - \alpha$. The resulting system would involve much larger products of region and propagation matrices

to form the eigenvalue problem (but this is okay since it is all done numerically), and the Bloch periodicity in this particular case would be five layers, instead of the original two alternating layers considered in this study.

It would be an interesting project to see whether increasing this unit cell from 5 to larger patterns yields any exotic phenomena to arise in our spatiotemporally modulated Drude medium.

5.2.4 Identification of topological features

Another potential direction is to explore the *topological properties* of the band structures and amplifying modes. By sweeping over a broader parameter space, varying not only the modulation speed, losses and obliqueness, but also the strength of the spatially periodic modulation, one can construct full dispersion *surfaces* and identify possible topological invariants (such as Chern numbers) associated with the bands.

Such studies are particularly relevant given the recent interest in topological photonics, where non-Hermitian effects (like gain/loss in our system) can yield rich phenomena like exceptional points and non-Hermitian skin effects, [24, 25]. In the context of space-time crystals, these topological features could provide robust amplifying edge modes, or other protected states, further expanding the practical and theoretical significance of the system.

References

[1] A. C. Harwood et al. "Superluminal synthetic motion with an optical space-time metasurface". In: PC13109 (Oct. 2024). DOI: 10.1117/12.3026893.

[2] J. C. Serra et al. "Particle-hole instabilities in photonic time-varying systems". In: *Opt. Mater. Express* 14.6 (June 2024), pp. 1459–1471. DOI: 10.1364/OME.521571.

[3] R. V. Craster and S. Guenneau. *Acoustic Metamaterials: Absorption, Cloaking, Imaging, Time-Modulated Media and Topological Crystals*. Second edition. Springer Series in Materials Science, 2024. ISBN: 9783031600142.

[4] V. M. Shalaev. "Optical negative-index metamaterials". In: *Nature Photonics* 1 (2007), pp. 41–48. DOI: 10.1038/nphoton.2006.49.

[5] D. J. Griffiths. *Introduction to electrodynamics*. Fifth edition. Cambridge: Cambridge University Press, 2024. ISBN: 9781009397759.

[6] F. R. Morgenthaler. "Velocity Modulation of Electromagnetic Waves". In: *IRE Transactions on Microwave Theory and Techniques* 6.2 (1958), pp. 167–172. DOI: 10.1109/TMTT.1958.1124533.

[7] E. S. Cassedy and A. A. Oliner. "Dispersion relations in time-space periodic media: Part I—Stable interactions". In: *Proceedings of the IEEE* 51.10 (1963), pp. 1342–1359. DOI: 10.1109/proc.1963.2566.

[8] E. S. Cassedy. "Dispersion relations in time-space periodic media: Part II—Unstable interactions". In: *Proceedings of the IEEE* 55.7 (1967), pp. 1154–1168. DOI: 10.1109/proc.1967.5775.

[9] J. Perini. "Periodically Loaded Transmission Lines". In: *IEEE Transactions on Microwave Theory and Techniques* 28.9 (1980), pp. 1029–1031. DOI: 10.1109/TMTT.1980.1130215.

[10] A. Smith et al. "Low noise microwave parametric amplifier". In: *IEEE Transactions on Magnetics* 21.2 (1985), pp. 1022–1028. DOI: 10.1109/TMAG.1985.1063665.

[11] C. Caloz and T. Itoh. *Electromagnetic Metamaterials: Transmission Line Theory and Microwave Applications*. Wiley, 2005.

[12] D. L. Sounas and A. Alù. "Non-reciprocal photonics based on time modulation". In: *Nature Photonics* 11 (2017), pp. 774–783. DOI: 10.1038/s41566-017-0051-x.

[13] P. Delplace, A. Gómez-León, and G. Platero. "Merging of Dirac points and Floquet topological transitions in ac-driven graphene". In: *Phys. Rev. B* 88 (24 Dec. 2013), p. 245422. DOI: 10.1103/PhysRevB.88.245422.

[14] M. S. Mirmoosa et al. "Time-Varying Reactive Elements for Extreme Accumulation of Electromagnetic Energy". In: *Phys. Rev. Appl.* 11 (1 Jan. 2019), p. 014024. DOI: 10.1103/PhysRevApplied.11.014024.

[15] M. C. Rechtsman et al. "Photonic Floquet topological insulators". In: *Nature* 496 (2013), pp. 196–200. DOI: 10.1038/nature12066.

[16] E. Galiffi et al. "Photonics of time-varying media". In: *Advanced Photonics* 4.1 (2022). DOI: https://doi.org/10.1117/1.AP.4.1.014002.

[17] Y. Lu et al. *Time-varying Nonlinear Effects in Terahertz Generation*. 2024. arXiv: 2409.07266 [physics.optics].

[18] V. M. Levkovskaya, A. V. Kharitonov, and S. S. Kharintsev. "Time-varying materials for analog optical computing". In: *J. Opt. Technol.* 91.5 (May 2024), pp. 293–299. DOI: 10.1364/JOT.91.000293.

[19] S. A. Maier. *Plasmonics: Fundamentals and Applications*. Springer Science, 2007. ISBN: 9780387331508.

[20] J. J. Sakurai and J. Napolitano. *Modern Quantum Mechanics*. 3rd. Approximation methods, including degenerate and near-degenerate perturbation theory. Cambridge University Press, 2021. Chap. 5.

[21] G. Cerullo and S. De Silvestri. "Ultrafast optical parametric amplifiers". In: *Review of Scientific Instruments* 74.1 (2003), pp. 1–18. DOI: 10.1063/1.1523642. eprint: https://pubs.aip.org/aip/rsi/article-pdf/74/1/1/19278885/1_1_online.pdf.

[22] L. D. Landau and E. M. Lifshitz. *Electrodynamics of Continuous Media*. 2nd. Vol. 8. Course of Theoretical Physics. Butterworth-Heinemann, 1984.

[23] B. Davies and L. Morini. "Super band gaps and periodic approximants of generalised Fibonacci tilings". In: *Proceedings of the Royal Society A* 480.2285 (Mar. 2024). DOI: 10.1098/rspa.2023.0663.

[24] L. Lu, J. D. Joannopoulos, and M. Soljačić. "Topological Photonics". In: *Nature Photon 8* (2014), pp. 821–829. DOI: 10.1038/nphoton.2014.248.

[25] T. Ozawa and H. M. Price. "Topological quantum matter in synthetic dimensions". In: *Nature Review Physics 1* (2019), pp. 349–357. DOI: 10.1038/s42254-019-0045-3.

[26] T. V. Raziman. *razimantv-scripts*. Unpublished, private code repository at Imperial College London. 2025.

[27] C. M. Bender, S. Boettcher, and S. Boettcher. "Real Spectra in Non-Hermitian Hamiltonians Having PT Symmetry". In: *Physical Review Letters* 80.24 (1998), p. 5243–5246. DOI: 10.1103/PhysRevLett.80.5243.

Appendix A

Appendix Chapter 1

A.1 Code implemented

Here we provide references to the computational resources used in this thesis. The primary codebase was developed by my supervisor, T. V. Raziman, and can be found at [26]. This code was crucial in implementing the numerical solutions for the transfer matrix approach, and visualising the dispersion profiles for varying parameters of the system.

In addition to this, I have developed my own supplementary code repository that builds on Raziman's work. My implementation includes further extensions to incorporate the oblique incidence modes, and includes additional code for generating new plots.

For those at Imperial, my repository may be accessed at:
`https://github.com/ImperialCollegeLondon/drude-spacetime-crystal`.

The combination of these resources forms the basis for the computational results presented in chapters 2 and 3, ensuring reproducibility and facilitating future exploration of these time-varying metamaterial systems.

A.2 Maxwell's equations

Maxwell's equations form the foundations of classical electrodynamics and describe how electric and magnetic fields evolve and interact with charges and currents. [5] has been the primary reference for all of the electromagnetism theory used throughout this work.

The general differential form of Maxwell's equations in a medium is given by:

$$\begin{aligned} \nabla \cdot \mathbf{E} &= \frac{\rho}{\varepsilon_0} \\ \nabla \cdot \mathbf{B} &= 0 \\ \nabla \times \mathbf{E} &= -\frac{\partial \mathbf{B}}{\partial t} \\ \nabla \times \mathbf{B} &= \mu_0 \mathbf{J} + \mu_0 \varepsilon_0 \frac{\partial \mathbf{E}}{\partial t} \end{aligned} \tag{A.1}$$

In a vacuum, there are no free charges or current, so $\rho = 0$ (the charge density), $\mathbf{J} = 0$ (the current density). The total electric field is equal to the sum of the field of the free charges and the field of the bound charges.

A bound charge density ρ_b is produced by an electric polarisation $\mathbf{P}$, specifically $\rho_b = -\nabla \cdot \mathbf{P}$.

$$\therefore \quad \rho = \rho_f + \rho_b = \rho_f - \nabla \cdot \mathbf{P}$$

Defining electric displacement $\mathbf{D}$ as $\mathbf{D} = \varepsilon_0 \mathbf{E} + \mathbf{P}$, yields the following alternative formulation of the first equation in (A.1).

$$\varepsilon_0 \nabla \cdot \mathbf{E} = \rho_f - \nabla \cdot \mathbf{P} \quad \Longrightarrow \quad \nabla \cdot \mathbf{D} = \rho_f$$

Furthermore, the current density $\mathbf{J}$ is the sum of the free currents $\mathbf{J}_f$, bound currents $\mathbf{J}_b$, and the polarization current $\mathbf{J}_p$.

A magnetic polarization $\mathbf{M}$ results in a bound current, specifically $\mathbf{J}_b = \nabla \times \mathbf{M}$, and since any change since any change in the electric polarization involves a flow of charge, we have $\mathbf{J}_p = \frac{\partial \mathbf{P}}{\partial t}$.

$$\therefore \quad \mathbf{J} = \mathbf{J}_f + \mathbf{J}_b + \mathbf{J}_p = \mathbf{J}_f + \nabla \times \mathbf{M} + \frac{\partial \mathbf{P}}{\partial t}$$

Defining the magnetic field intensity $\mathbf{H}$ as $\mathbf{H} = \frac{1}{\mu_0}\mathbf{B} - \mathbf{M}$, yields the following alternative formulation of the fourth equation in (A.1).

$$\frac{1}{\mu_0} \nabla \times \mathbf{B} = \mathbf{J}_f + \nabla \times \mathbf{M} + \frac{\partial \mathbf{P}}{\partial t} + \varepsilon_0 \frac{\partial E}{\partial t} \quad \Longrightarrow \quad \nabla \times \mathbf{H} = \mathbf{J}_f + \frac{\partial \mathbf{D}}{\partial t}$$

A.2.1 The wave equation in a vacuum

Assuming the setting of a vacuum with $\rho = 0$, $\mathbf{J} = 0$. Then we have $\nabla \cdot \mathbf{E} = 0$ and $\nabla \times \mathbf{B} = \mu_0 \varepsilon_0 \frac{\partial \mathbf{E}}{\partial t}$.

Considering the curl of equation 3 in (A.1); $\nabla \times (\nabla \times \mathbf{E}) = \nabla \times \left(-\frac{\partial \mathbf{B}}{\partial t}\right)$.

But from multivariable calculus identities and using the fact that $\nabla \cdot \mathbf{E} = 0$ we also have

$$\nabla \times (\nabla \times \mathbf{E}) = \nabla (\nabla \cdot \mathbf{E}) - \nabla^2 \mathbf{E} = -\nabla^2 \mathbf{E}$$

Furthermore, considering the curl of $-\frac{\partial \mathbf{B}}{\partial t}$, and using $\nabla \times \mathbf{B} = \mu_0 \varepsilon_0 \frac{\partial \mathbf{E}}{\partial t}$, we obtain

$$\nabla \times \left(-\frac{\partial \mathbf{B}}{\partial t} \right) = -\frac{\partial}{\partial t} \left(\nabla \times \mathbf{B} \right) = -\mu_0 \varepsilon_0 \frac{\partial^2 \mathbf{E}}{\partial t^2}$$

As a result, we obtain the classical wave equation.

$$\frac{\partial^2 \mathbf{E}}{\partial t^2} - \frac{1}{\mu_0 \varepsilon_0} \nabla^2 \mathbf{E} = 0 \tag{A.2}$$

By considering a similar argument with $\nabla \times (\nabla \times \mathbf{B}) = \nabla \times \left(\mu_0 \varepsilon_0 \frac{\partial \mathbf{E}}{\partial t} \right)$, the wave equation with the magnetic field $\mathbf{B}$ may also be obtained.

$$\frac{\partial^2 \mathbf{B}}{\partial t^2} - \frac{1}{\mu_0 \varepsilon_0} \nabla^2 \mathbf{B} = 0 \tag{A.3}$$

A.2.2 Dispersion relation in a linear dispersionless medium

Consider the (macroscopic) Maxwell's equations in a medium.

$$\begin{aligned} \nabla \cdot \mathbf{D} &= \rho_f \\ \nabla \cdot \mathbf{B} &= 0 \\ \nabla \times \mathbf{E} &= -\frac{\partial \mathbf{B}}{\partial t} \\ \nabla \times \mathbf{H} &= \mathbf{J}_f + \frac{\partial \mathbf{D}}{\partial t} \end{aligned} \tag{A.4}$$

Since we are in a linear medium, the following relations hold, $\mathbf{D} = \varepsilon \mathbf{E}$ and $\mathbf{B} = \mu_0 \mathbf{H}$.

Moreover, assume time-harmonic solutions (which is a common thing to do in many practical scenarios and something we will do in our setup later on), that is $\mathbf{E}(\mathbf{r}, t) = \mathbf{E}_0 e^{i(\mathbf{k} \cdot \mathbf{r} - \omega t)}$ and $\mathbf{B}(\mathbf{r}, t) = \mathbf{B}_0 e^{i(\mathbf{k} \cdot \mathbf{r} - \omega t)}$.

Apply the time-harmonic solutions to the third equation in (A.4), $\nabla \times \mathbf{E} = -\frac{\partial \mathbf{B}}{\partial t}$.

$$\begin{aligned} \nabla \times \mathbf{E} &= i\mathbf{k} \times \mathbf{E}_0 e^{i(\mathbf{k} \cdot \mathbf{r} - \omega t)} \\ -\frac{\partial}{\partial t} \left(\mathbf{B}_0 e^{i(\mathbf{k} \cdot \mathbf{r} - \omega t)} \right) &= i\omega \mathbf{B}_0 e^{i(\mathbf{k} \cdot \mathbf{r} - \omega t)} \\ \implies \mathbf{k} \times \mathbf{E}_0 &= \omega \mathbf{B}_0 \end{aligned}$$

Similarly, applying the time-harmonic solutions to the fourth equation in (A.4), $\nabla \times \left(\frac{\mathbf{1}}{\mu_0} \mathbf{B} \right) =$

$\mathbf{J}_f + \frac{\partial \varepsilon \mathbf{E}}{\partial t}$.

$$\nabla \times \left(\frac{\mathbf{1}}{\mu_\mathbf{0}} \mathbf{B} \right) = i \frac{1}{\mu_0} \mathbf{k} \times \mathbf{B}_0 e^{i(\mathbf{k}\cdot\mathbf{r} - \omega t)}$$
$$\mathbf{J}_f + \varepsilon \frac{\partial \mathbf{E}}{\partial t} = \mathbf{J}_f - i\varepsilon\omega \mathbf{E}_0 e^{i(\mathbf{k}\cdot\mathbf{r} - \omega t)}$$

$$\implies \mathbf{k} \times \mathbf{B}_0 = -\mu_0 \varepsilon \omega \mathbf{E}_0$$

where the last implication above follows from equating the imaginary parts of the two equations above it.

Consider $\mathbf{k} \times (\mathbf{k} \times \mathbf{E}_0) = (\mathbf{k} \cdot \mathbf{E})\,\mathbf{k} - (\mathbf{k} \cdot \mathbf{k})\,\mathbf{E}_0$, by the vector triple product, and we can write $\mathbf{k} \cdot \mathbf{k} = k^2$.

But also, $\mathbf{k} \times \mathbf{E}_0 = \omega \mathbf{B}_0$ and $\mathbf{k} \times (\omega \mathbf{B}_0) = \omega(\mathbf{k} \times \mathbf{B}_0) = -\mu_0 \varepsilon \omega^2 \mathbf{E}_0$.

$$\therefore \ \left(k^2 - \mu_0 \varepsilon \omega^2\right) \mathbf{E}_0 = (\mathbf{k} \cdot \mathbf{E})\,\mathbf{k}$$

Now, in our linear medium $\mathbf{k}$ and $\mathbf{E}$ are perpendicular if and only if the free charge density in the region is zero, $\rho_f = 0$, since

$$i\mathbf{k} \cdot \mathbf{E} = \nabla \cdot \mathbf{E} = \frac{1}{\varepsilon} \nabla \cdot \mathbf{D} = \frac{\rho_f}{\varepsilon}$$

Hence, if we take $\rho_f = 0$, then $k^2 - \mu_0 \varepsilon \omega^2 = 0 \implies \omega = \pm \frac{1}{\sqrt{\mu_0 \varepsilon}} k$, the appropriate linear dispersion relation. The constant $\frac{1}{\mu_0 \varepsilon}$ is equal to c, the speed of light, so it is also common to write this dispersion relation as $\omega = \pm ck$.

In our Drude model, we will be working with a dispersive medium instead, and so the dispersion relation there is not as simple.

Appendix B

Appendix Chapter 2

B.1 Fields in a non-time-varying Drude medium

Considering a non-time-varying Drude medium, we may assume the fields in the medium to be of the form $E = f(z)e^{-i\omega t}$, $H = g(z)e^{-i\omega t}$, $v = h(z)e^{-i\omega t}$ (*i.e* time-harmonic since there is no time modulation). From this, we obtain

$$\begin{aligned} f'(z) &= i\omega g(z) \\ g'(z) &= -h(z) + i\omega f(z) \\ i\omega h(z) &= \Gamma h(z) - \delta f(z) \end{aligned}$$

$$\therefore \; f''(z) + \underbrace{\left(\omega^2 - \frac{\omega}{\omega + i\Gamma}\delta\right)}_{\text{call this } k^2(\omega)} f(z) = 0$$

$$\implies f(z) = f_+ \exp\left(ik_\omega z\right) + f_- \exp\left(-ik_\omega z\right)$$

From this $f(z)$, we can then obtain $g(z)$ and $h(z)$.

$$\begin{aligned} g(z) &= \frac{1}{i\omega} f'(z) = \frac{k}{\omega}\left(f_+ \exp\left(ik_\omega z\right) - f_- \exp\left(-ik_\omega z\right)\right) \\ h(z) &= \frac{\delta}{\Gamma - i\omega} f(z) = \frac{\delta}{\Gamma - i\omega}\left(f_+ \exp\left((ik_\omega z\right) + f_- \exp\left(-ik_\omega z\right)\right) \end{aligned}$$

This therefore shows that fields of this form have a z-dependence of $\sim e^{ikz}$.

B.2 Subluminal dispersion profile for $c = 0.7$ and complex plane ω tracking

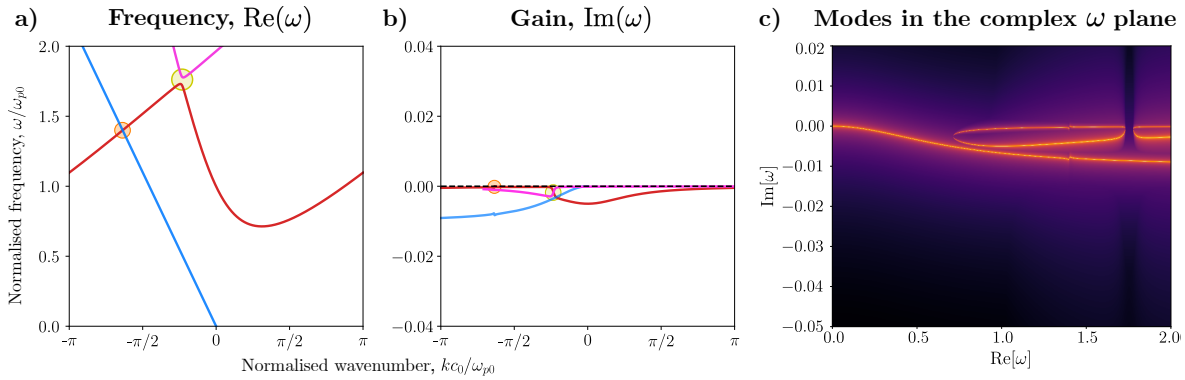

Figure B.1: **Subluminal normal waves dispersion and complex ω plane branches.** The system under consideration has parameters $\delta = [1.25, 0.75]$, $\Gamma = 0.01$, and $c = 0.7$. a), b) Band structures for the system show that the extent of amplification (orange circle in b)) is greatly reduced compared to the $c = 0.97$ case (see Figure 2.3). The amplification occurs at a smaller wavenumber, consistent with the reduced shearing of the homogeneous branches at $c = 0.7$, leading to the branch crossing shifting to a lower κ_z. In the yellow circle, the opening of the Drude band gap is visible, although the gap here is significantly smaller than for $c = 0.97$. c) Admissible mode branches are plotted in the complex ω-plane, obtained by scanning across the relevant (ω, κ) grid and checking the mode condition. This view highlights the presence of the complex frequency solutions in the system.

Appendix C

Appendix Chapter 3

C.1 Recovering the TE Drude dispersion relation

Consider the first three equations in (3.3) with $c = 0$.

$$\begin{aligned} -\omega E_{y_0} - i v_{y_0} &= k_z H_{x_0} - k_x H_{z_0} \\ \omega H_{x_0} &= -k_z E_{y_0} \\ \omega H_{z_0} &= k_x E_{y_0} \end{aligned}$$

$$\implies k_z H_{x_0} - k_x H_{z_0} = -\frac{k_z^2}{\omega} E - \frac{k_x^2}{\omega} E = -\frac{\overbrace{\left(k_x^2 + k_z^2\right)}^{k_0^2}}{\omega}$$

$$\therefore -\omega E_{y_0} - i v_{y_0} = -\frac{k_0^2}{\omega^2} \implies v_{y_0} = i\left(\omega - \frac{k_0^2}{\omega}\right) E_{y_0}$$

But now the fourth equation in (3.3) tells us

$$v_{y_0} = \frac{\delta}{\Gamma - i\omega} E_{y_0}$$

Combining these to eliminate v_{y_0}, E_{y_0} (since these are non-zero) yields

$$k_0^2 - \omega^2 = \frac{i\delta\omega}{\Gamma - i\omega} \implies k_0^2 = \omega^2\left(1 - \frac{\delta}{\omega^2 + i\Gamma\omega}\right)$$

which is the appropriate Drude dispersion relation.

C.2 Fields in a non-time-varying Drude medium for TE- and TM-polarised waves

TE

Restricting ourselves to a single-layer in the medium, we may assume the fields are of the form $E_y = e(z)e^{i(k_x x-\omega t)}$, $H_x = h_x(z)e^{i(k_x x-\omega t)}$, $H_z = h_z(z)e^{i(k_x x-\omega t)}$, $v_y = v(z)e^{i(k_x x-\omega t)}$ (where we are assuming harmonic forms in x and t as there would be no modulation in these dimensions in a single-layer). The first four equations in (3.1) imply solutions for our fields have a dependence of the form $\exp\{i\,(k_x x + k_z z - \omega t)\}$. We can show this explicitly.

$$\begin{aligned} h_x'(z) - ik_x h_z(z) &= v(z) - i\omega e(z) \\ e'(z) &= -i\omega h_x(z) \\ ik_x e(z) &= i\omega h_z(z) \\ -i\omega v(z) &= -\Gamma v(z) + \delta e(z) \end{aligned}$$

This implies that $e''(z) + \left(\omega^2 - k_x^2 + \frac{i\delta\omega}{\Gamma - i\omega}\right) e(z) = 0$, which means that $e(z) = E_0 e^{ik_z(\omega)z}$, and similar results then follow from this for the other fields.

TM

Considering a single-layer in the non-time-varying setup, we may assume the fields in the medium are of the form $H_y = f(z)e^{i(k_x x-\omega t)}$, $E_x = g(z)e^{i(k_x x-\omega t)}$, $E_z = h(z)e^{i(k_x x-\omega t)}$, $v_x = v_1(z)e^{i(k_x x-\omega t)}$, $v_z = v_2(z)e^{i(k_x x-\omega t)}$.

$$\begin{aligned} -i\omega f(z) &= ik_x h(z) - g'(z) \\ f'(z) &= -v_1(z) + i\omega g(z) \\ ik_x f(z) &= v_2(z) - i\omega h(z) \\ -i\omega v_1(z) &= -\Gamma v_1(z) + \delta g(z) \\ -i\omega v_2(z) &= -\Gamma v_2(z) + \delta h(z) \end{aligned}$$

$$\implies v_1(z) = \frac{\delta}{\Gamma - i\omega} g(z), \;\; v_2(z) = \frac{\delta}{\Gamma - i\omega} h(z)$$

From these, we can obtain two equations in $g(z)$ and $h(z)$ as below.

$$\begin{aligned} g''(z) - ik_x h'(z) &= \left(-\omega^2 + \frac{\delta\omega}{\Gamma\omega + i\omega^2}\right) g(z) \\ ik_x g'(z) + k_x^2 h(z) &= \left(\omega^2 - \frac{\delta\omega}{\Gamma\omega + i\omega^2}\right) h(z) \end{aligned}$$

This leads to a solution of the form $g(z) = C\exp\{ik_z(\omega)z\}$, and hence $f(z)$ and $h(z)$ have similar forms as well, just adjusted by some factors.

C.3 Example of an evanescent TE mode

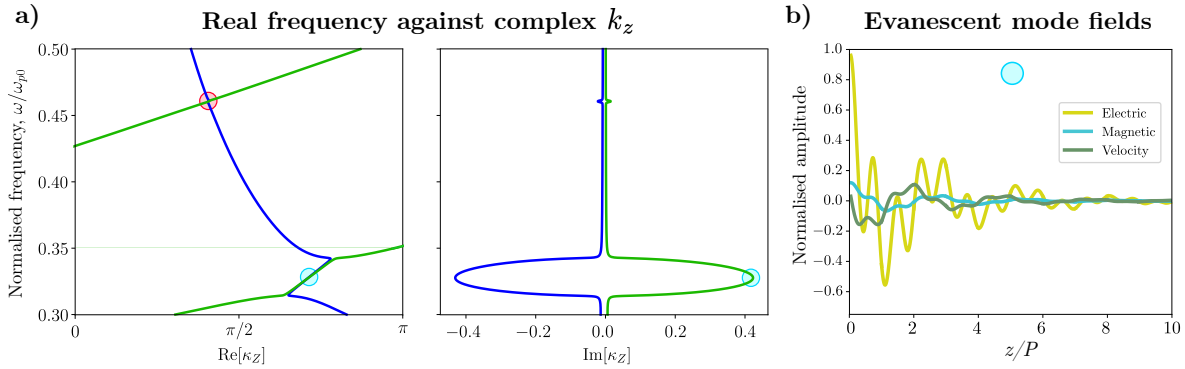

Figure C.1: **Example of an evanescent mode for TE polarised waves.** The system under consideration has parameters $\delta = [1.25, 0.75]$, $\Gamma = 0.01$, $c = 0.97$, $k_x = 0.5$. a) Band structure showing real frequency against complex wavenumber. The highlighted red and blue circles indicate points where the real parts of κ_z coincide but the imaginary parts diverge, forming a pair of complex conjugate wavenumbers. This divergence in the imaginary parts of κ_z is a signature of evanescent mode formation, reminiscent of $\mathcal{PT}$-symmetric-like branch-point behaviour in non-Hermitian systems, [27]. b) Field profile of the TE mode at the blue circle from a), demonstrating an evanescent character with the electric field dominating the mode structure. The rapid decay of the field along z highlights the non-propagating, spatially localised nature of the evanescent wave in this parameter regime.

Appendix D

Appendix Chapter 4

D.1 Special case of the inner product with $\Gamma = 0$

When $\Gamma = 0$, our normalizing factor C_i takes a much simpler form.

$$C_i = \frac{1}{\sqrt{1 + \frac{\kappa^2}{|\omega_i'|^2} + \frac{1}{|\omega_i'^2|}}}$$

But, recall from the Drude dispersion relation that $\kappa^2 = \omega^2\left(1 - \frac{\delta}{\omega^2}\right)$ (when $\Gamma = 0$), but $\delta = 1$ in this unperturbed setting and so the relation simplifies to $\omega^2 = \kappa^2 + 1$.

$$\therefore \;\; C_i = \frac{1}{\sqrt{1 + \frac{|\omega_i|^2}{|\omega_i'|^2}}} = \sqrt{\frac{|\omega_i + ck|^2}{|\omega_i|^2 + |\omega_i + ck|^2}}$$

For the $c = 0$ case, we can see that this reduces to $C_i = \frac{1}{\sqrt{2}}$.

D.2 Deriving expressions for the linear and hyperbolic branches

We begin with everyone's favourite Drude dispersion relation as the basis for deriving the branch approximations.

$$k^2 = \omega'^2\left(1 - \frac{1}{\omega'^2 + i\Gamma\omega'}\right)$$

Here, $\omega' = \omega + ck$.

Linear branch

From the analysis of the homogeneous cubic, we know that one of the solutions is at $\omega' = 0$ and this corresponds to the linear branch and hence this has non-zero imaginary component only. As a result, we may write $\omega' = -i\beta$ for some $\beta \in \mathbb{R}$ which we know is small.

$$\therefore \;\; k^2 = \frac{\beta}{\Gamma - \beta} - \beta^2 \sim \frac{\beta}{\Gamma - \beta} \quad \text{(since } \beta \text{ small)}$$

This implies that $\beta = \Gamma \cdot \frac{k^2}{k^2+1}$, and so we have our linear branch as follows writing $\omega' = \omega + ck$.

$$\omega_l = -ck - i\Gamma \frac{k^2}{k^2+1}$$

Hyperbolic branch

From the Drude dispersion relation, if the solution is not the linear branch, then the other two solutions are the positive and negative hyperbola. Since Γ is small, we may write this as,

$$k^2 = \omega'^2 - \frac{\omega'}{\omega' + i\Gamma} = \omega'^2 - \frac{1}{1 + \frac{i\Gamma}{\omega'}} \sim \omega'^2 - 1 + \frac{i\Gamma}{\omega}$$

Now, ω' has a real component ω'^r and an imaginary component ω'^i, and so we may write $\omega' = \omega'^r + i\omega'^i$, where ω'^i is small (so we can take ${\omega'^i}^2$ as negligible).

$$\therefore \;\; k^2 + 1 = {\omega'^r}^2 + 2i\omega'^r\omega'^i + \frac{i\Gamma}{\omega'^r\left(1 + \frac{i\omega'^i}{\omega'^r}\right)} = {\omega'^r}^2 + i\left(2\omega'^r\omega'^i + \frac{\Gamma}{\omega'^r}\right)$$

Since the LHS above is real, we can compare real and imaginary parts to obtain, $\omega'^r = \sqrt{k^2+1}$ and $\omega'^i = -\frac{\Gamma}{2{\omega'^r}^2} = -\frac{\Gamma}{2(k^2+1)}$. So, we have our hyperbolic branch as follows.

$$\omega = \sqrt{k^2+1} - ck - \frac{i\Gamma}{2(k^2+1)}$$

D.3 Approximating the normalising factor for the hyperbolic mode (normal incidence, subluminal amplification)

We have $(1 + H_h H_h^* + v_h v_h^*)^{-\frac{1}{2}}$, where $H_h = \frac{2k_h(k_h^2+1)}{2(k_h^2+1)^{\frac{3}{2}} - i\Gamma}$ and $v_h = \frac{2i\left(k_h^2+1\right)}{2\left(k_h^2+1\right)^{\frac{3}{2}} + i\Gamma\left(2\left(k_h^2+1\right)-1\right)}$.

In our setting, k_h is fixed as the value of k at the crossing when folded once in the Brillouin zone, and so we use the approximation $k_h \approx 2\pi - 0.27 \approx 6$. This reduces H_h and v_h down significantly.

$$H_h \approx \frac{444}{450 - i\Gamma}\,, \;\; v_h \approx \frac{74i}{450 + 73i\Gamma}$$

$$\begin{aligned}\therefore \;\; (1 + H_h H_h^* + v_h v_h^*)^{-\frac{1}{2}} &= \left(1 + \frac{444}{450 - i\Gamma} \cdot \frac{444}{450 + i\Gamma} + \frac{74i}{450 + 73i\Gamma} \cdot \frac{-74i}{450 - 73i\Gamma}\right) \\ &\approx \sqrt{\frac{5000\Gamma^4 + 1\text{e}9\Gamma^2 + 4\text{e}10}{5000\Gamma^4 + 2\text{e}9\Gamma^2 + 8\text{e}10}} \sim \frac{1}{\sqrt{2}}\end{aligned}$$

The above algebraic computation is not hard to check. The last approximation of $\frac{1}{\sqrt{2}}$ follows since Γ is small and the numerator and denominator in the square root are of the same polynomial order.

D.4 Algebra for the product of the overlap integrals (normal incidence, subluminal amplification)

Observe that the only varying parameter in our mode expressions is Γ, and since k is fixed, focusing on the crossing point, we have $k_h \approx 2\pi - 0.27 \approx 6$ and $k_l \approx -0.25$. Applying this approximation to the modes derived,

$$v_l^* = \sqrt{\frac{0.25^2}{0.25^2\Gamma^2 + 1.0625}}\,,\;\; E_h = \frac{1}{\sqrt{2}}\,,\;\; v_h^* = \frac{-74i\,(450 + 73i\Gamma)}{\sqrt{2}\,(450^2 + 73^2\Gamma^2)}\,,\;\; E_l = \sqrt{\frac{0.25^2}{0.25^2\Gamma^2 + 1.0625}}\cdot\frac{\Gamma}{1.0625}$$

$$\implies P_{lh}P_{hl} = \frac{-2\alpha^2}{\pi^2}\frac{0.25^2\Gamma}{1.0625\,(0.25^2\Gamma^2 + 1.0625)}\frac{(73\cdot 74\Gamma - 74\cdot 450i)}{(450^2 + 73^2\Gamma^2)}$$

To make the approximation in $P_{lh}P_{hl}$ simpler, it is clear that the real part of the expression is a factor of Γ times the imaginary part, and so it is *much smaller* (since Γ small). So, we may approximate $P_{lh}P_{hl}$ with just its imaginary part.

$$P_{lh}P_{hl} \approx \frac{2i\alpha^2}{\pi^2}\frac{74\cdot 450\cdot 0.25^2\Gamma}{1.0625\,(0.25^2\Gamma^2 + 1.0625)\,(450^2 + 73^2\Gamma^2)}$$

The numerical values in this expression can be significantly approximated, such as $1.0625 \approx 1$ and $74{\cdot}450{\cdot}0.25^2 \approx 2000$. Moreover, we apply Taylor's series to $\frac{1}{450^2+73^2\Gamma^2} \approx 5\text{e}{-6}\left(1 - 0.03\Gamma^2\right)$.

$$\implies \frac{\pi^2}{2i\alpha^2}P_{lh}P_{hl} \approx \frac{0.01\Gamma\left(1 - 0.03\Gamma^2\right)}{0.25^2\Gamma^2 + 1} = \frac{0.16\Gamma\left(1 - 0.03\Gamma^2\right)}{\Gamma^2 + 16} \sim \frac{\Gamma\left(1 - 0.01\Gamma^2\right)}{10\left(\Gamma^2 + 10\right)}$$

D.5 Algebraic derivation for superluminal gain with respect to obliqueness

We start with working out Ψ_{positive} and Ψ_{negative}, in the standard way.

$$\Psi_{\text{positive}} \sim \frac{1}{\sqrt{2\left(k_x^2 + k_{z_p}^2 + 1\right)}}\begin{pmatrix}\omega_p'\\ -k_{z_p}\\ k_x\\ i\end{pmatrix}\,,\;\; \Psi_{\text{negative}} \sim \frac{1}{\sqrt{2\left(k_x^2 + k_{z_n}^2 + 2\right)}}\begin{pmatrix}\omega_n'\\ -k_{z_n}\\ k_x\\ i\end{pmatrix}$$

Letting $\eta_p = k_x^2 + k_{z_p}^2 + 1$ (and similar for η_n) for ease of notation (so $\omega_p' = \frac{2\eta_p^{\frac{3}{2}} - i\Gamma}{2\eta_p}$ and similar for ω_n'). With this notation, the overlap integrals P_{pn}, P_{np} may be written,

$$P_{pn} = \frac{-2\alpha}{\pi}\cdot\frac{-i}{\sqrt{2\eta_p}}\cdot\frac{2\eta_n^{\frac{3}{2}} - i\Gamma}{2\sqrt{2}\eta_n^{\frac{3}{2}}}\,,\;\; P_{np} = \frac{2\alpha}{\pi}\cdot\frac{-i}{\sqrt{2\eta_n}}\cdot\frac{2\eta_p^{\frac{3}{2}} - i\Gamma}{2\sqrt{2}\eta_p^{\frac{3}{2}}}\,.$$

It can be seen that the real part of $P_{pn}P_{np}$ behaves like $\frac{1}{\sqrt{\eta_n\eta_p}}$ (with some pre-factors), however, as discussed for the approximations in previous sections, we care only about the

magnitude of the imaginary part of $P_{pn}P_{np}$. This is given below.

$$P_{pn}P_{np} = \frac{\alpha^2}{4\pi^2}\frac{\left(2\eta_n^{\frac{3}{2}} - i\Gamma\right)\left(2\eta_p^{\frac{3}{2}} - i\Gamma\right)}{\eta_p^2\eta_n^2} \sim \frac{-i\alpha^2\Gamma\left(\eta_n^{\frac{3}{2}} + \eta_p^{\frac{3}{2}}\right)}{2\pi^2\left(\eta_n^2 + \eta_p^2\right)} \quad \text{(in imaginary part)}$$

Here, we have a factor of $-i$ instead of the usual i, as seen in previous cases, however this is okay since we can take the minus sign in (4.4), and so we want to maximise the negative imaginary contribution in the square root for maximum positive imaginary part in the overall perturbed frequency. We can look at the profile of this gain as a function of the obliqueness k_x (substituting the approximation of $k_{z_p} = 0.66$, $k_{z_n} = 0.66 - 2\pi$, so $k_{z_p}^2 + 1 \approx 1.4$, $k_{z_n}^2 + 1 \approx 32.6$).

$$f(k_x) = \frac{\alpha^2\Gamma\left((k_x^2 + 32.6)^{\frac{3}{2}} + (k_x^2 + 1.4)^{\frac{3}{2}}\right)}{2\pi^2\left((k_x^2 + 32.6)^2 + (k_x^2 + 1.4)^2\right)} \tag{D.1}$$

One can simplify the terms in this even more by taking $1.4 \approx 1$ and $32.6 \approx 30$, and for even more simplification, one can notice that the numerator is dominated by $(k_x + 32.6)^{\frac{3}{2}}$ and the denominator is dominated by $(k_x + 32.6)^2$, for reasonable values of k_x. Hence, this can also be approximated like $\sim \frac{1}{\sqrt{k_x^2+1}}$.